NASA CR-145067

RESEARCH AND DEVELOPMENT FOR IMPROVED LEAD-SALT DIODE LASERS

Final Report

Prepared under Contract No. NAS1-12979

By

Jack F. Butler

ARTHUR D. LITTLE, INC.

Cambridge, Mass. 02140

for

TABLE OF CONTENTS

SECTION 1

INTRODUCTION

1.1 Program Goals

A number of planned NASA programs related to global and regional monitoring or remote sensing of atmospheric constituents or pollutants are centered around the use of Pb-salt tunable diode lasers.[1-6] The central interest in these lasers is related to their narrow linewidth and wavelength tunability. Their emission frequency can be selected within a wide spectral range by choice of composition (see F 1-1), while lasers of fixed composition can be tuned during operation by varying bias current or other parameters.[7] Emission lines can thus be adjusted to match gas absorption lines optimized with respect to absorption strength and interfering species. The following specific application areas for Pb-salt tunable diode lasers have been identified and analyzed for use on air or space platforms as remote and in-situ sensors of atmospheric pollution:

- A double-ended aircraft or balloon-based sensor for performing in-situ measurements of atmospheric pollution, with particular relevance to the environmental impact of high flying aircraft. The system comprises a tunable diode laser transmitter, retroreflector, and receiver, and encompasses a 10-meter path length.[3,5]

- A single-ended remote sensor in a solar viewing mode using a laser heterodyne spectrometer to measure minor constituents in the upper troposphere and stratosphere. In this case, the tunable diode laser acts as a laser local oscillator for obtaining various stratospheric constituents.[7]

- A single-ended remote sensor in a nadir viewing mode using a laser heterodyne spectrometer to measure atmospheric constituents in the troposphere and stratosphere by detecting the upwelling thermal radiance of the earth and the atmosphere.[2]

SECTION 1

INTRODUCTION

1.1 Program Goals

A number of planned NASA programs related to global and regional monitoring or remote sensing of atmospheric constituents or pollutants are centered around the use of Pb-salt tunable diode lasers.[1-6] The central interest in these lasers is related to their narrow linewidth and wavelength tunability. Their emission frequency can be selected within a wide spectral range by choice of composition (see F 1-1), while lasers of fixed composition can be tuned during operation by varying bias current or other parameters.[7] Emission lines can thus be adjusted to match gas absorption lines optimized with respect to absorption strength and interfering species. The following specific application areas for Pb-salt tunable diode lasers have been identified and analyzed for use on air or space platforms as remote and in-situ sensors of atmospheric pollution:

- A double-ended aircraft or balloon-based sensor for performing in-situ measurements of atmospheric pollution, with particular relevance to the environmental impact of high flying aircraft. The system comprises a tunable diode laser transmitter, retroreflector, and receiver, and encompasses a 10-meter path length.[3,5]

- A single-ended remote sensor in a solar viewing mode using a laser heterodyne spectrometer to measure minor constituents in the upper troposphere and stratosphere. In this case, the tunable diode laser acts as a laser local oscillator for obtaining various stratospheric constituents.[7]

- A single-ended remote sensor in a nadir viewing mode using a laser heterodyne spectrometer to measure atmospheric constituents in the troposphere and stratosphere by detecting the upwelling thermal radiance of the earth and the atmosphere.[2]

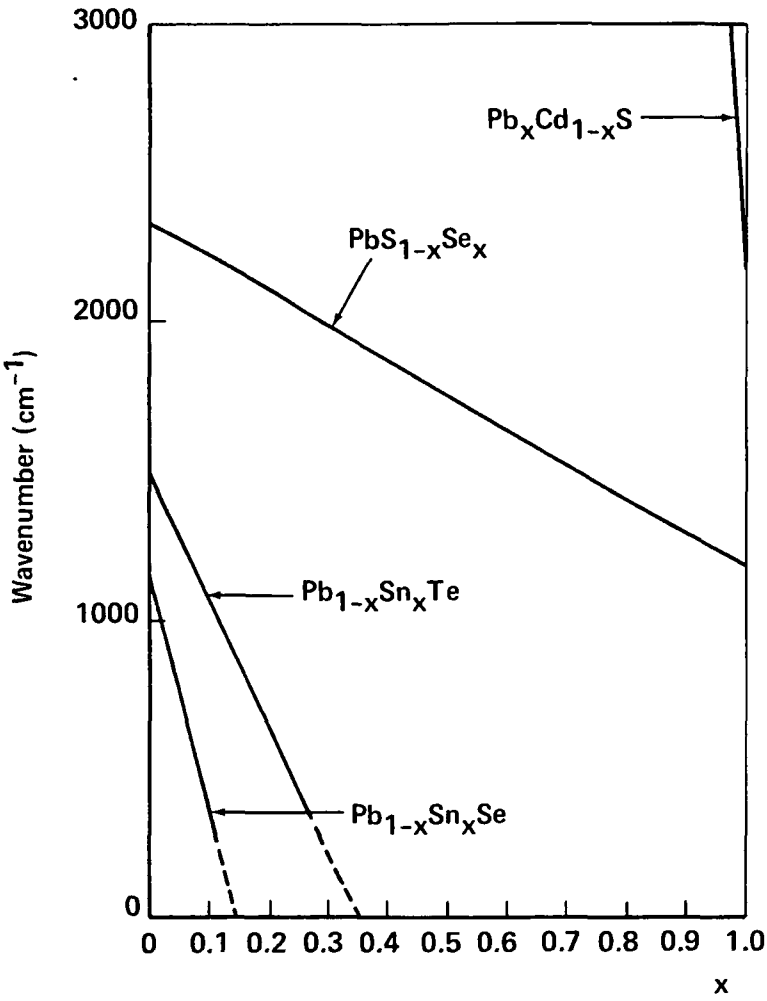

FIGURE 1–1 COMPOSITION DEPENDENCE OF EMISSION FREQUENCY FOR VARIOUS Pb-SALT COMPOUND LASERS

- A single-ended remote sensor with a laser transmitter and heterodyne receiver on a mobile platform and using differential absorption measurements with earth as a diffuse reflector. In this case, measurement of the total column concentration of pollutants or constituents in the lower 5-kilometer region of the troposphere is measured.[4]

These applications require power outputs considerably in excess of those of routinely available tunable diode lasers. Specifically, whereas analysis has indicated requirements of 1 to 10 milliwatts in a single mode for the above applications, commercially available Pb-salt diode lasers have generally exhibited 0.1 milliwatt per mode at best. Accordingly, a primary purpose of this program was to substantially increase the power output achievable on a routine basis for certain compositions of Pb-salt lasers; the goal was a single-mode, single-ended power output greater than 1 milliwatt. The program concentrated on $PbS_{1-x}Se_x$, with x tailored to match emission wavelengths with absorption bands of CO ($\approx$ 4.7 μm) and NO ($\approx$ 5.3 μm).

1.2 Technical Approach

The initial stage of the program was devoted to crystal growth and other efforts related to materials preparation. The ADL growth, annealing and diffusion procedures were adapted and optimized to yield lasers for the desired spectral regions. A new vapor-phase crystal-growing technique was developed to produce larger crystals and yielded single crystals with areas up to 5 cm^2. Diode lasers were fabricated by conventional methods at this stage to provide a means of measuring crystal composition and evaluating crystal quality.

An important aspect of the program was the development of improved diode laser structures in which parasitic side-bounce and internally reflected modes are greatly reduced or eliminated. The existence of parasitic modes significantly restricts the power output of diode lasers. Two approaches to eliminating such modes were taken, (1) development of an angle-lapped

structure, and (2) utilization of a stripe geometry configuration. Other factors investigated during the program included pn-junction profile optimization, end-face metallization, end-face polishing and damage associated with standard laser packaging methods.

1.3 Summary of Results

The principal results of the program are as follows:

- Single-mode, single-ended output powers in excess of 1 milliwatt were achieved, with more than 8 milliwatts being observed with exceptional devices.

- Tuning range was varied by pn-junction depth control. Overall tuning ranges were varied from approximately 20 cm^{-1} to 100 cm^{-1}, with single-mode tuning ranges up to 5 cm^{-1} being observed in the second case.

- Laser crystal damage resulting from the standard packaging method was noted, and a new package investigated to overcome this problem.

- End-face metallization experiments yielded values for loss coefficient ($\alpha \approx 6.4$ cm^{-1}) and gain factor ($\beta \approx 0.06$ cm/amp) and suggested methods for further improvements in output power.

- The crystal composition of Pb $S_{1-x}Se_x$ could be significantly altered (x-value increased) by annealing at temperatures as low as 600°C in the presence of a Se vapor source. This effect has not been previously reported and has important consequences related to Pb-salt laser fabrication.

SECTION 2

CRYSTAL GROWTH AND MATERIALS PREPARATION

Single crystals were grown by the vapor phase recrystallization method, in routine use in the ADL laboratories, and by an unseeded transport technique developed to produce crystals of larger size than produced by vapor phase recrystallization. Materials were evaluated through evaluation of laser operating characteristics.

2.1 Vapor Phase Recrystallization

The starting elements were of the highest purity obtainable from commercial sources and, excepting sulfur, were zone-refined with over 50 passes under flowing, high-purity H_2 gas. The elements were weighed out to form mixtures of the desired composition which were stoichiometric with respect to metal/nonmetal proportions. Five-gram charges were typically used. These mixtures were reacted in evacuated, sealed quartz ampoules at temperatures approximately 50°C above the melting temperature.

Quartz tubes and ampoules used in all materials operations were cleaned, etched and vacuum-baked overnight at 1100°C, using a nitrogen trapped, oil diffusion pump. Thorough vacuum baking of ampoules was found to be necessary for reproducible crystal growth.

The reacted, polycrystalline ingot was sealed in evacuated ampoules for regrowth into single crystal form. In the growth apparatus (F 2-1), the 1/2-inch-diameter ampoule is open to a long, closed capillary tube extending into the room temperature region. The capillary is designed to remove volatile impurities and fix the stoichiometric composition. Transport of material provides a self-sealing mechanism for the tube. The ampoule is situated in an Na heat pipe which reduces the temperature gradient along the ampoule to below the measurement limits of ± 0.5°C. The growth temperature was 800°C.

Crystal growth times were typically three days. A programmed cooldown of 40°C/hour was used after growth. Growth occurs vertically from the

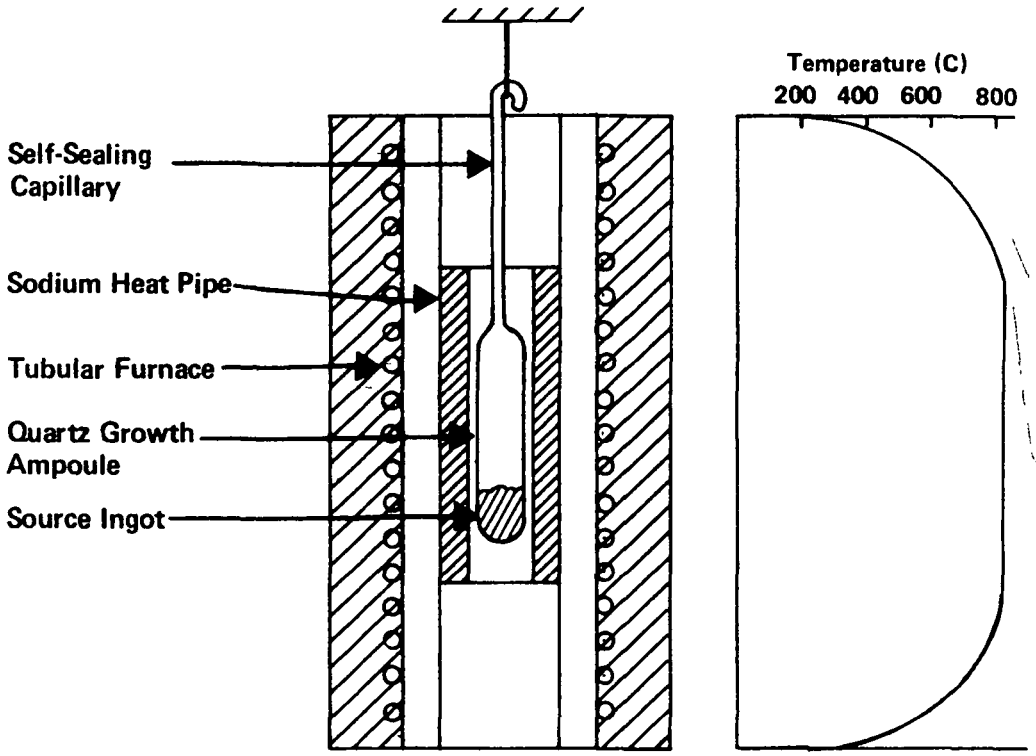

FIGURE 2–1 APPARATUS FOR VAPOR PHASE RECRYSTALLIZATION GROWTH OF Pb-SALTS

starting source and one to three crystals with well-defined (100) facets are generally produced. Facet dimensions are typically 3-5 mm on a side. This method of crystal growth has several advantageous features, (1) driving away of volatile impurities before growth, (2) elimination of contact of the grown crystal with the quartz walls, and (3) relative simplicity.

Crystals were grown by this procedure for source mole compositions of $PbS_{0.800}Se_{0.200}$, $PbS_{0.640}Se_{0.360}$ and $PbS_{0.615}Se_{0.385}$. Subsequent measurements of laser emission frequencies established that $x = 0.200$ and $x = 0.385$ are appropriate compositions for obtaining emission wavelengths in the 4.7 μm and 5.3 μm regions, for monitoring the CO and NO molecules, respectively.

2.2 Vapor Phase Transport

Initial program plans called for the use of standard photoprocessing methods in the fabrication of stripe geometry devices. Since the small crystals produced by the vapor phase recrystallization method are not easily manipulated in photoprocessing steps, a method of vapor phase transport was developed to produce crystals of larger size. The 1-inch diameter growth ampoule was shaped to a 30° cone at the tip end, with a self-sealing capillary extending from the tip. A 50-gram prereacted charge was sealed in the evacuated ampoule. Growth was carried out with the ampoule situated virtually in a temperature gradient of approximately 1°C/cm and at a temperature of 1,000°C. Growth time was four days, and the ampoule was cooled in the furnace at a rate of 20°C/hour. The entire 50-gram charge generally transported, forming a single crystal attached to the tip. F 2-2 shows a typical crystal of PbSSe grown by this method.

2.3 Annealing

After growth, crystals grown by vapor phase recrystallization were annealed at 450°C in the unopened growth ampoules for periods exceeding a week. Slices of the larger, transported crystals were similarly annealed in sealed, evacuated quartz tubes before being processed into

FIGURE 2–2 SINGLE CRYSTAL OF $PbS_{0.8}Se_{0.2}$ GROWN BY UNSEEDED VAPOR TRANSPORT METHOD

devices. Experience has shown that such annealing significantly improves diode laser performance. The annealed crystals were n-type with carrier concentrations in the order of 2×10^{18} cm^{-3}. According to Strauss and Harman[8], crystals with this concentration are near metal saturation at the annealing temperature of 450°C.

2.4 Fabrication of Diode Lasers for Materials Characterization

A number of lasers were fabricated for materials characterization. Thus, the laser emission wavelength provides the most meaningful measurement of crystal composition, while factors such as the nature and density of foreign impurities and defects are of interest in the present effort only to the extent that they affect laser performance.

Pn-junctions were formed in annealed n-type crystals by heating them in the presence of a Se saturated PbSe diffusion source. In these preliminary runs, the diffusions were performed in sealed quartz tubes at a temperature of 525°C for a period of one hour. This produced a junction depth of approximately 100 μm. Both p and n surfaces of diffused crystals were metallized with electroplated Au to a thickness of approximately 0.2 μm[9]. An 0.2 μm layer of Pt was electroplated onto the Au and a final layer of In, about 10 μm thick, was electroplated onto the Pt. Commercial plating baths were used. Dice were formed by cleaving. The laser crystals were assembled in the standard ADL package, with the p-type skin bonded to the metal heat sink and a C-bend contact attached to the top surface. All contacts were made at room temperature by relying on the cold welding properties of In. F 2-3 shows a line drawing of the laser structure, while F 2-4 shows photographs of an actual assembled laser. After assembly, the lasers were given a preliminary evaluation by measurement of the 77°K volt-ampere characteristic and threshold current and power output at 4.2K. F 2-5 presents typical volt-ampere curves for a PbSSe laser at a temperature of 77°K. The significant feature in F 2-5 is the incremented slope in the linear region at forward bias, which indicates a series resistance of about 25 milliohms. A low series resistance is important to prevent overheating during operation of the laser; series resistance greater than

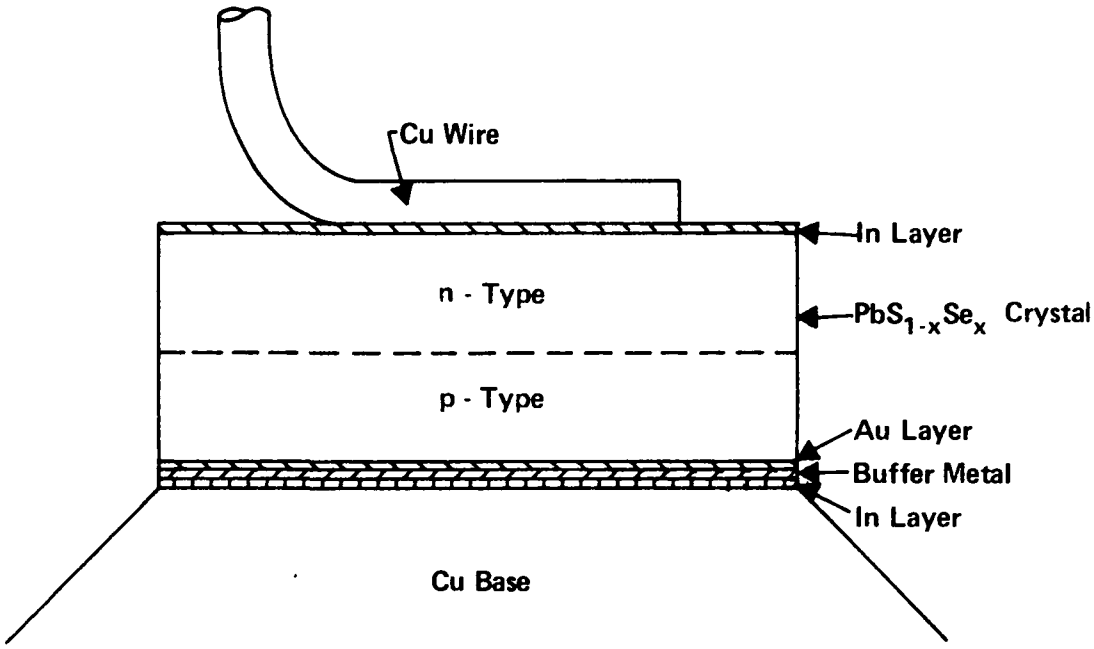

FIGURE 2–3 CONCEPTUAL DRAWING OF DIODE LASER STRUCTURE

FIGURE 2–4a PHOTOGRAPH OF A CONVENTIONAL PbS Se DIODE LASER IN THE C-BEND PACKAGE

FIGURE 2–4b CLOSEUP VIEW OF A PbS Se DIODE LASER

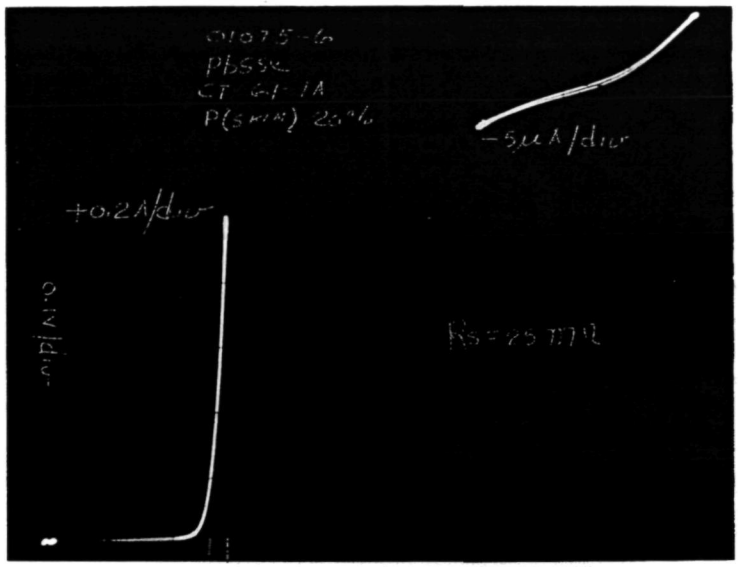

FIGURE 2–5 VOLT-AMPERE CHARACTERISTICS OF A $PbS_{0.8}Se_{0.2}$ DIODE LASER AT 77° K. HORIZONTAL SCALE IS 0.1 V/div. VERTICAL SCALE IS 0.2 A/div. FOR FORWARD BIAS (BOTTOM-LEFT) AND 5 μA/div. FOR REVERSE BIAS (UPPER-RIGHT).

about 0.2 ohm prevents CW operation of the lasers. For threshold and power measurements, the lasers were mounted on the end of a "dipstick", situated to illuminate a calibrated Ge:Cu detector in close proximity. The dip-stick was inserted into a liquid He storage vessel for the measurement. T 2-1 gives dipstick data for a number of diode lasers fabricated from material grown by vapor phase recrystallization. T 2-1 also includes spectral data taken by measurements to be described below.

2.5 Diode Laser Characterization

For spectral measurement the lasers were installed on the cold finger of a liquid N_2-jacketed liquid He dewar equipped to hold four lasers simultaneously. The lasers were DC biased with a Model SCPS-II power supply manufactured by Arthur D. Little, Inc. A BaF_2 window allowed transmission of the infrared radiation. The radiation was collected with an f/1, BaF_2 lens and focused onto the entrance slit of a grating monochromator having a resolution of about 0.2 cm^{-1} at minimum slit width. A variable speed chopper was mounted behind the entrance slit. The output of the monochromator was focused onto a 1 mm^2 HgCdTe detector manufactured by ADL. The detector output was then fed into a lock-in amplifier and displayed on an XY recorder.

F 2-6 shows emission spectra for a typical PbSSe diode laser (TDL-05074-1) at various DC bias currents. As indicated the spectra of PbSSe diode lasers generally exhibit multi-mode behavior 10-20% above threshold. The indicated width of the modes is determined by the resolution limit of the grating monochromator. Current tuning curves were traced out by generating a number of emission spectra such as those of F 2-6 and noting the turn-on and turn-off currents of individual modes. The tuning ranges of several lasers investigated in this manner are included in T 2-1. F 2-7 shows a tuning characteristic of a typical device.

The tuning characteristics of F 2-7 are noteworthy for their broad range. The overall tuning range of over 100 cm^{-1} and single mode tuning ranges up to 5 cm^{-1} evident in F 2-7 are significantly greater than previously

TABLE 2-1

DIPSTICK THRESHOLD & POWER MEASUREMENTS

Growth Number	Source X	Device Number	Threshold Current (ampere)	Power Output at $2xI_{th}$ (microwatts)	Emission Frequency Range for $I \leq 2$ amps (cm^{-1})
CT-58	0.200	03224-1	0.16	30	
		03224-2	0.18	30	
		03224-3	0.22	125	2085-2206
		03224-4	0.12	45	2098-2164
		03224-5	0.16	75	
		03224-6	0.26	37	
CT-75	0.360	05154-1	0.24	60	
		05154-2	0.28	70	1937-1955
		05154-3	0.30	75	
		05154-4	0.14	35	
		05154-5	0.34	80	
		05154-7	0.30	125	1947-1954
CT-66	0.385	05034-4	0.06	30	
		05034-5	0.14	400	
		05034-6	0.14	250	
		05034-7	0.08	75	1902-1932
		05034-8	0.26	275	1896-1941

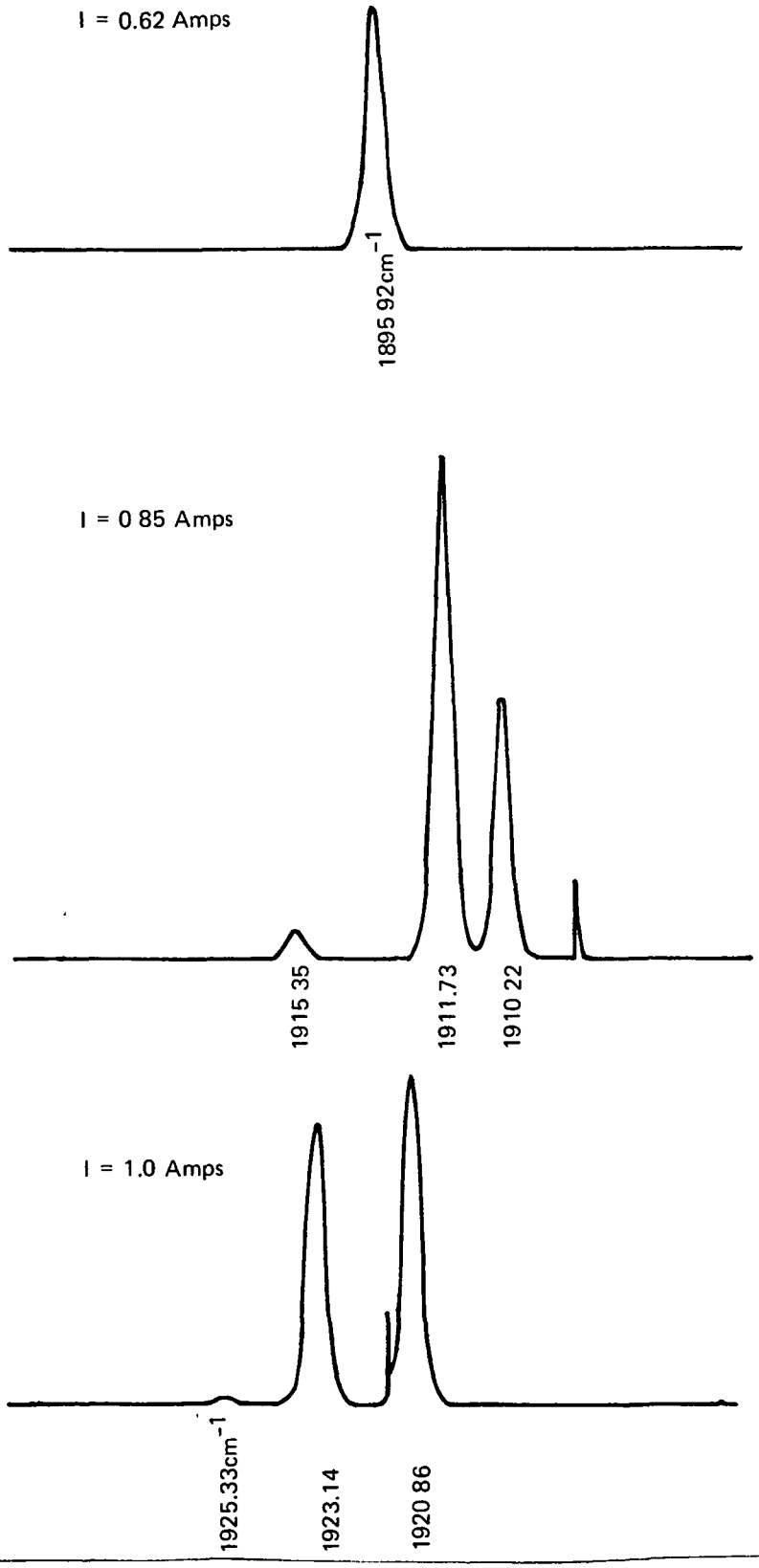

FIGURE 2–6 EMISSION SPECTRA OF A $PbS_{.615}Se_{.385}$ DIODE LASER (TDL–05074–1) AT VARIOUS BIAS CURRENTS. HORIZONTAL SCALE UNITS IN cm^{-1}

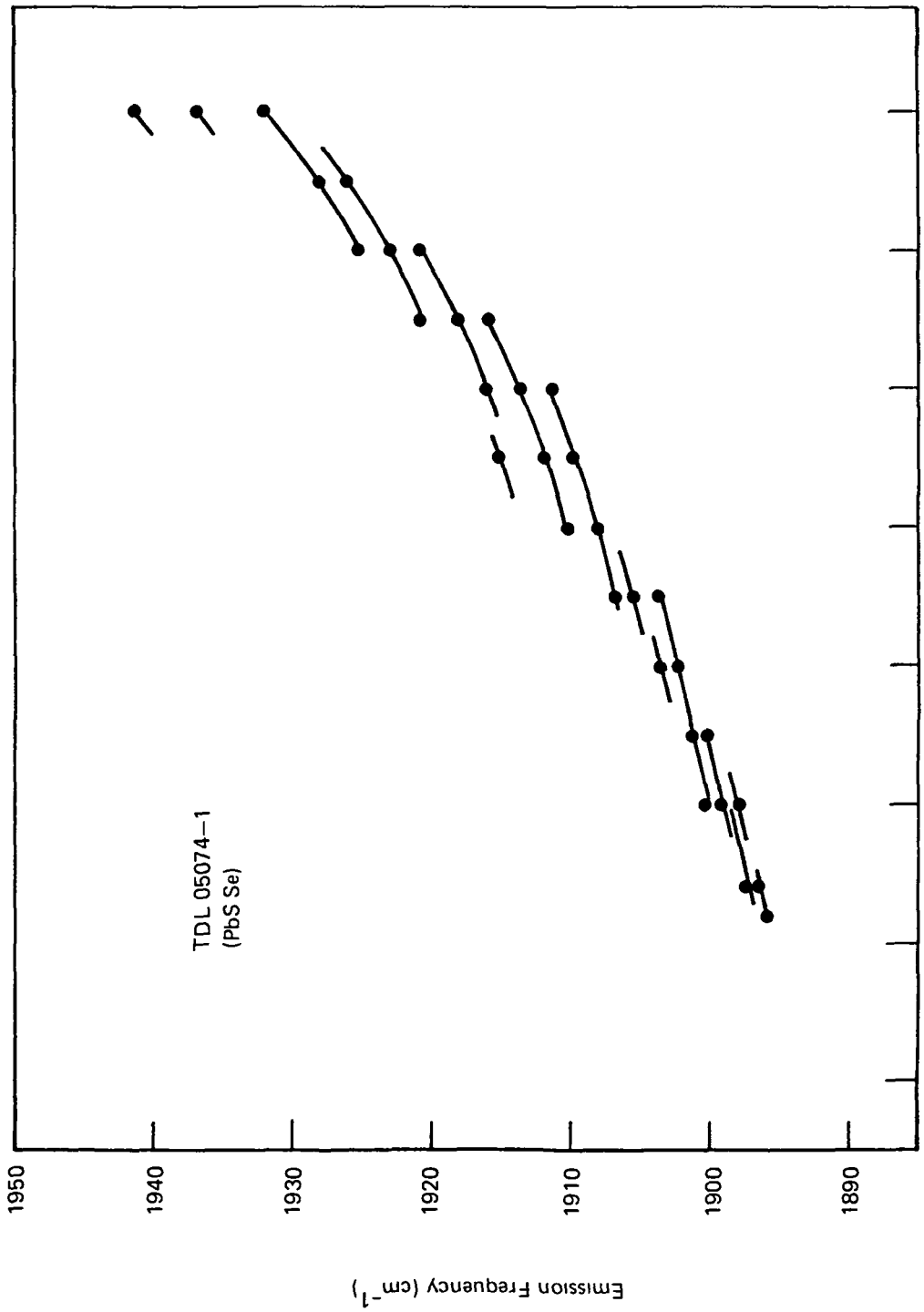

FIGURE 2–7 CURRENT TUNING CHARACTERISTICS OF TDL–05074–1

reported for current tuned diode lasers operating with a fixed heat sink temperature[10]. A wide tuning range is particularly advantageous for high-resolution spectral measurements since it allows a correspondingly wide range to be investigated with a single laser. For monitoring applications where the laser is operating at essentially a fixed spectral position, a wide tuning range (with a corresponding high tuning rate) is undesirable because it places higher stability requirements on the biasing power supply. The current tuning rate is determined by factors such as the electrical resistance of the laser crystal and contacts, the thermal conductivity of the crystal and the distance of the pn-junction from the heat sink. In the present lasers, the high tuning rate is directly related to the large junction depth ($\gtrsim$ 100 μm); the wide tuning range is additionally related to the fact that the lasers are able to operate in the CW mode at temperatures substantially higher than their heat sink. Tuning rates can be greatly reduced by decreasing the junction depth.

The power output of the lasers was measured with a pyroelectric sensor loaned by Dr. R. J. Phelan of the National Bureau of Standards Laboratories, Boulder, Colorado. The area of the sensor active element was 1 cm^2, allowing a large fraction of the radiation to be directly captured from most lasers. Power measurements were made with the lasers pulse-biased at a 400 Hz repetition rate and a pulse width of 2 microseconds. F 2-8 shows results of low duty cycle pulsed measurements of a typical diode laser. A significant feature of the curve in F 2-8 is the linear behavior over a wide region above threshold. This indicates saturation of the internal quantum efficiency. Another indication of high internal quantum efficiency is shown in the 4.2°K V-I curve of F 2-9. The pronounced kink in the slope is apparent at the threshold current for laser action. This effect can be explained by a significant decrease in the average carrier lifetime at the onset of laser action, which would only occur if a large fraction of the injected carriers took part in the stimulated emission process.

The temperature dependence of threshold current was measured with the lasers mounted in a liquid-flow He cryostat equipped with a heater and

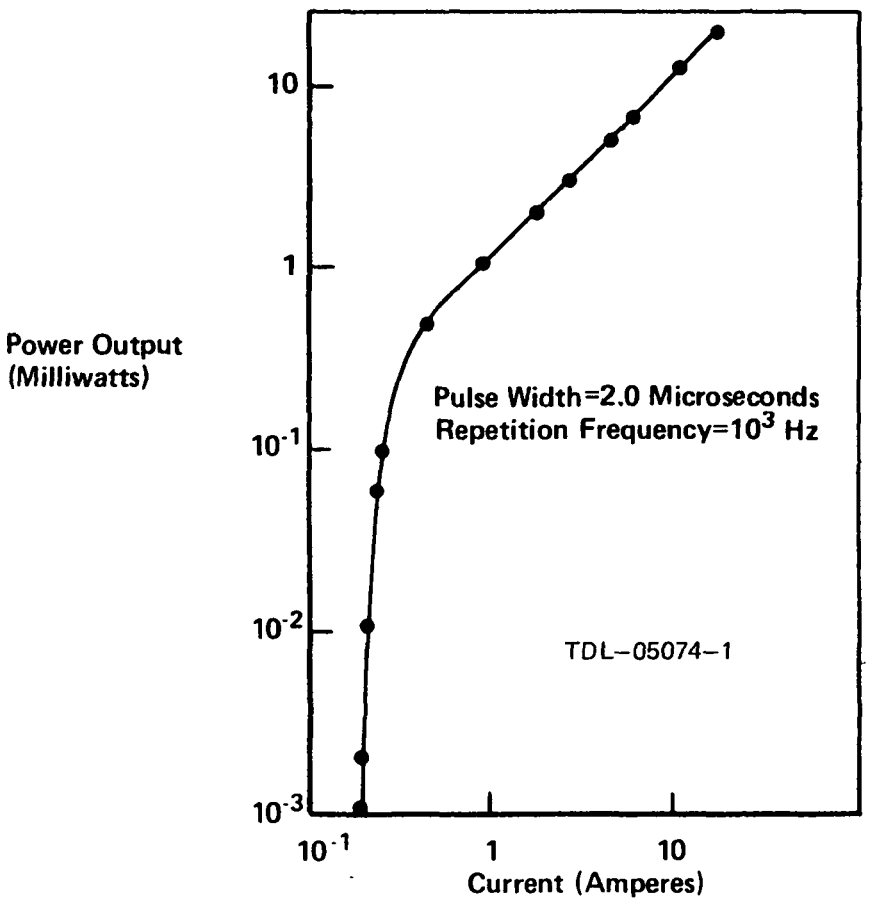

FIGURE 2–8 DEPENDENCE OF OUTPUT POWER ON BIAS CURRENT FOR A $PbS_{0.8}Se_{0.2}$ DIODE LASER AT 4.2 K

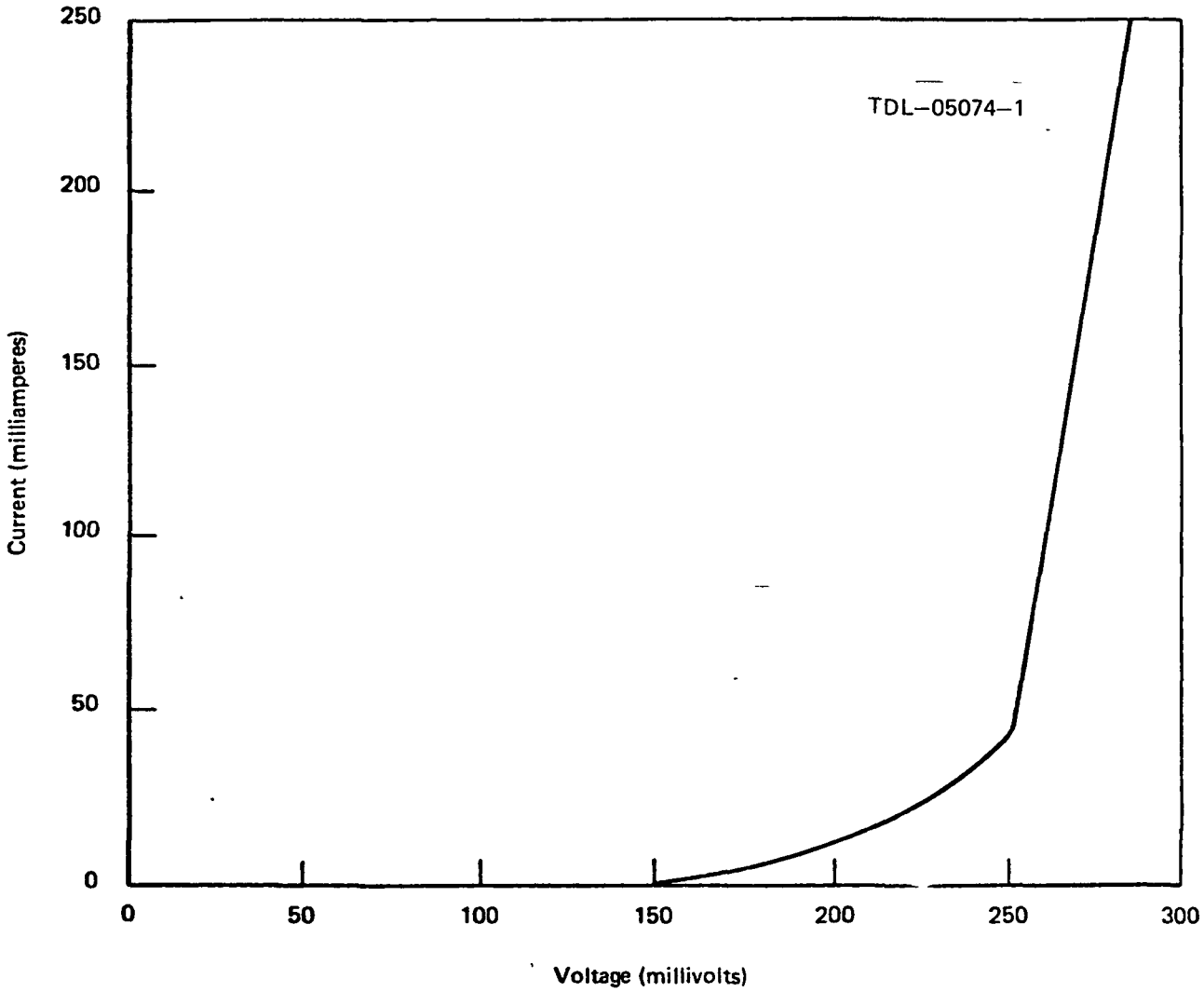

FIGURE 2–9 VOLT-AMPERE CHARACTERISTICS OF A $PbS_{1-x}Se_x$ DIODE LASER AT 10 K ILLUSTRATING AN EFFECT DUE TO THE ONSET OF LASER ACTION

a feedback temperature control unit. The temperature could be varied from 4.2°K to room temperature. F 2-10 shows the dependence of threshold current on temperature for a typical device measured in the pulsed mode of operation. The increase of threshold current with temperature is slow, and pulsed laser action has been observed up to 100°K. In exceptional devices, CW operation was possible up to 65°K. From these results, it seems reasonable to postulate that CW operation to above 77°K will be achieved with further improvements in heat sinking and junction depth optimization.

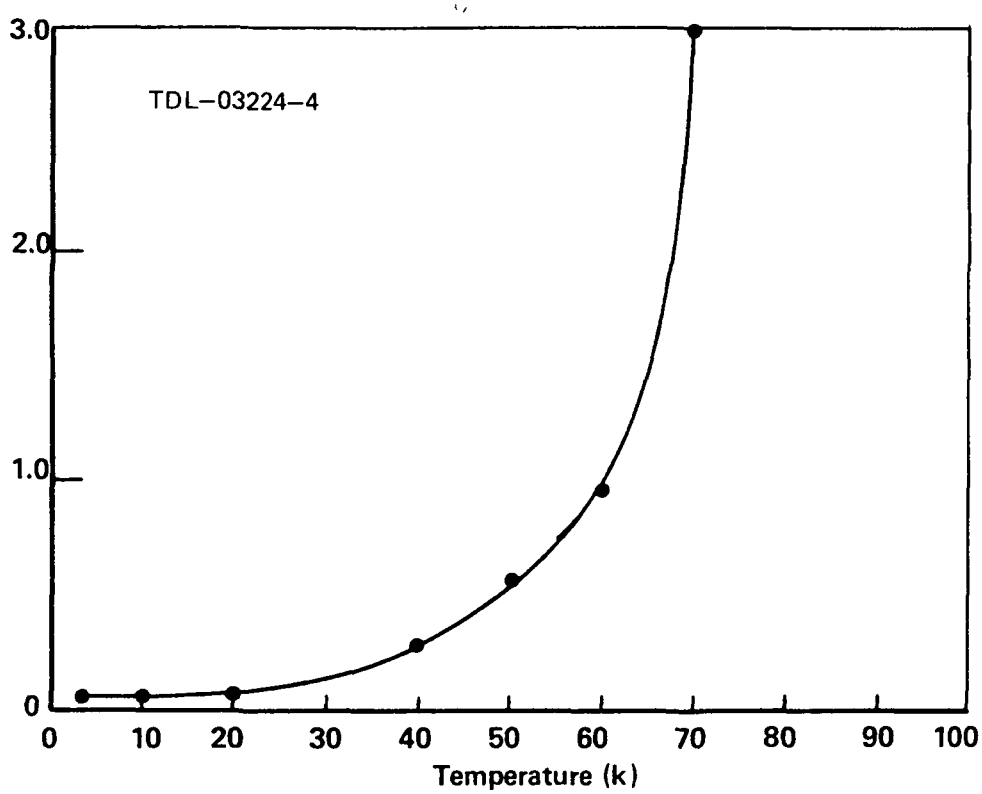

FIGURE 2–10 DEPENDENCE OF THRESHOLD CURRENT ON TEMPERATURE FOR A $PbS_{0.8}Se_{0.2}$ DIODE LASER

SECTION 3

IMPROVEMENTS IN DEVICE FABRICATION

An important aspect of this program was developing reproducible and reliable methods to fabricate diode lasers that minimize parasitic side-bounce and internally reflected modes. Two approaches were successfully followed to achieve this goal, angle-lapping and the use of stripe geometry. In addition, experiments related to junction depth optimization, end-face metallization and end-face polishing were carried out. Microphotographic observation of laser crystals provided information on crystal damage.

3.1 Angle-Lapped Diode Lasers

As discussed in Section 1, an important goal of this program was to produce laser structures which eliminate parasitic side-bounce and internally reflected modes from the laser cavity. The original approach was to develop a stripe geometry configuration, and this has been successfully accomplished. An alternative approach, using an angle-lapping technique, has also been developed. The angle-lap method has advantages of simplicity in that it does not require diffusion masking or junction insulation steps.

In the angle-lapped diode laser, one, or both, of the long, unmetallized faces perpendicular to the laser end-faces is lapped at an angle such that incident radiation is reflected away from the pn-junction plane. Thus, laser oscillations associated with reflections from the side walls cannot build up. The fabrication procedures for angle-lapped lasers are essentially identical to those for the standard lasers discussed in Section 2, with the addition that lapping and etching steps are added to produce the angled side wall structure.

The laser crystals were mounted on specially prepared quartz lapping fixtures. Standard semiconductor lapping procedures are not generally applicable to IV-VI compound lasers because lapping damage to the crystals strongly degrades properties related to emission of radiation. A procedure was developed based on lapping with progressively smaller grid sizes

(#600 to 2 μm) and finishing with an etch-polishing step in which no grid is employed. Several etching compounds were investigated for use in the final step. The chosen etchant was chromium trioxide in water. Surfaces produced by this method showed etch pit densities no higher than those of surfaces exposed by careful cleaving (10^4-10^5 cm^{-2}). F 3-1 is a line drawing showing the angled structure.

Diodes were characterized by the methods described in Section 2. For lasers fabricated from the same crystal, angle-lapped devices had somewhat higher threshold currents and considerably higher power outputs than standard devices. As an example, T 3-1 presents threshold and power output data for several angle-lapped lasers compared with similar data from standard lasers prepared from the same crystal growth run. F 3-2 shows curves of single-ended power output vs. bias current for two exceptional devices whose CW power exceeded 10 milliwatts overall. Note that the power output ranges from 1.5 to 2.6 milliwatts for the angle-lapped devices, but from only 0.03 to 0.125 milliwatts for the standard lasers. Thus a power increase of more than a factor of ten was achieved by the angle-lapping procedure. Threshold currents for the angle-lapped devices are seen to be consistently higher than the standard devices. This is to be expected, because the objectional circulating modes in the standard devices generally have high Q resulting from the fact that they involve total internal reflections within the crystal. Spectral measurements for laser TDL 08134-6 (F 3-3) indicate that most of the power is concentrated in only a few modes at higher current levels. This diode produced up to 5 milliwatts in a single mode. As shown in F 3-4, laser TDL 08094-16 has a poorer mode structure: the maximum observed single-mode CW power was approximately 2 milliwatts. The poorer mode quality of TDL 08094-16 may be related to I^2R heating of the device with bias current. This factor apparently accounts for the rapid drop in power at relatively low currents and the large current tuning rate indicated in Figures 3-4, which shows a shift in emission frequency of approximately 200 cm^{-1} with current increased from 0.4 to 0.9 amperes. The principal component of electrical resistance in a Pb-salt diode laser is the metal-semiconductor contact resistance, which

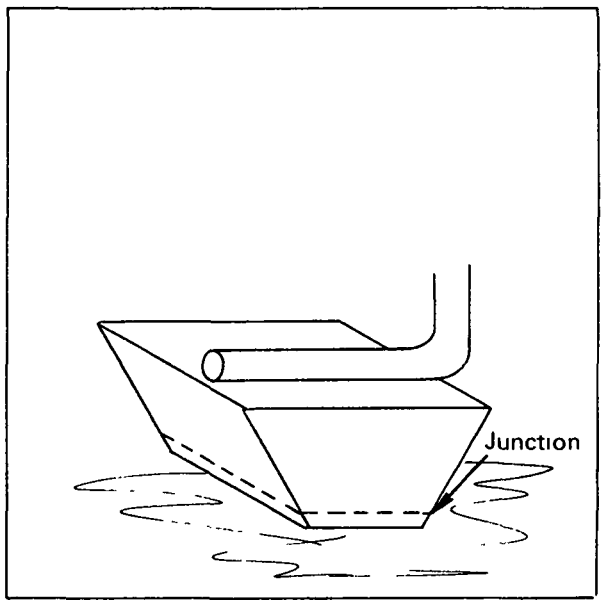

FIGURE 3–1 LINE DRAWING OF AN ANGLE-LAPPED DIODE LASER

TABLE 3-1

CHARACTERIZATION DATA FOR $PbS_{1-x}Se_x$ DIODE LASERS

Fabrication Method	Diode Laser Number	Threshold Current (Ampere)	Power Output at $2I_{th}$ (milliwatts)
Angle Lap	08134-1	0.28	2.0
	08134-2	0.31	1.5
	08134-3	0.60	2.2
	08134-4	0.20	2.6
Standard (Table 2-1)	03124-1	0.16	0.030
	03124-2	0.18	0.030
	03124-3	0.22	0.125
	03124-4	0.12	0.045
	03124-5	0.16	0.075
	03124-6	0.26	0.037

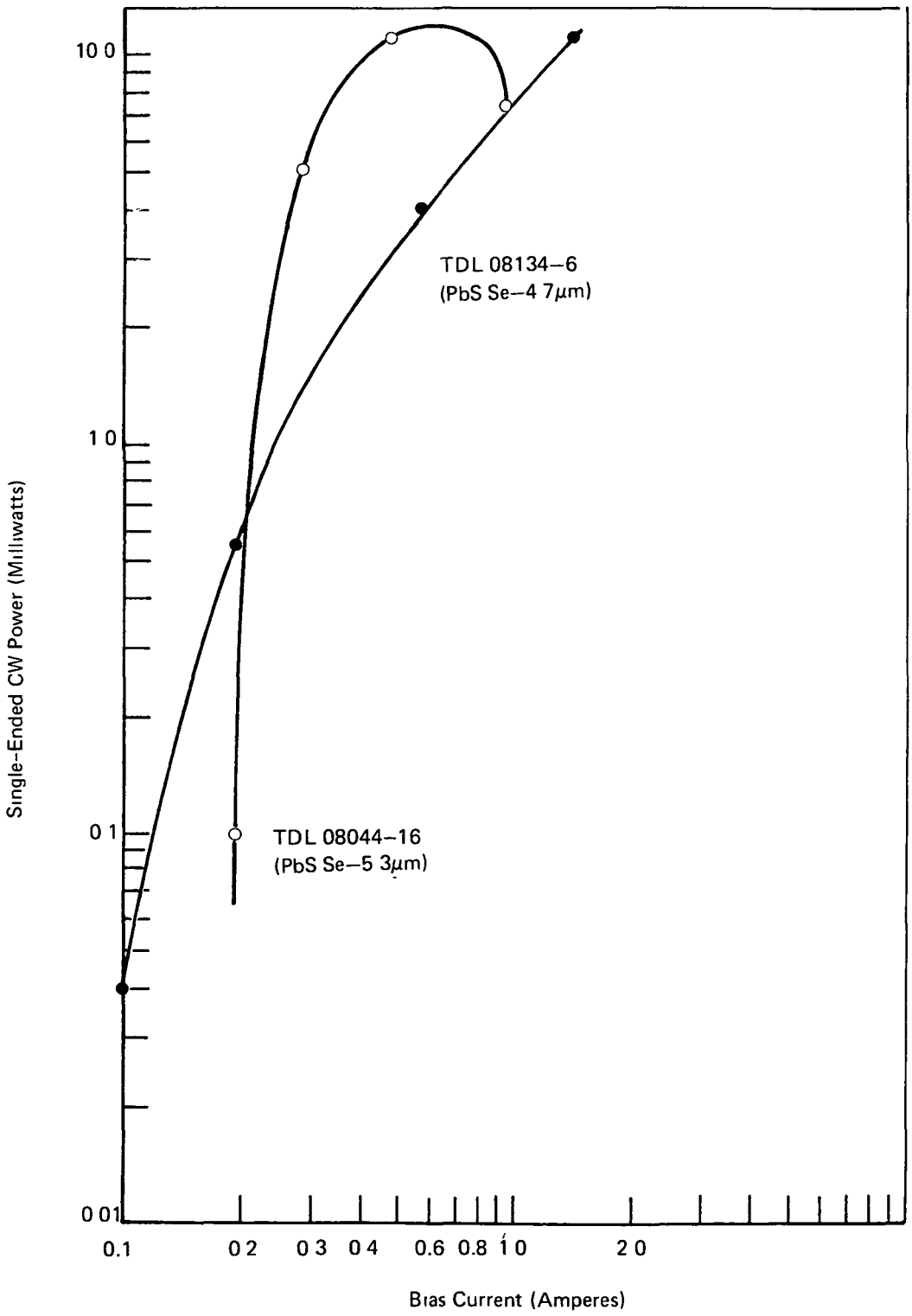

FIGURE 3–2 DEPENDENCE OF SINGLE-ENDED, CW POWER OUTPUT ON CURRENT FOR TWO PbS Se DIODE LASERS

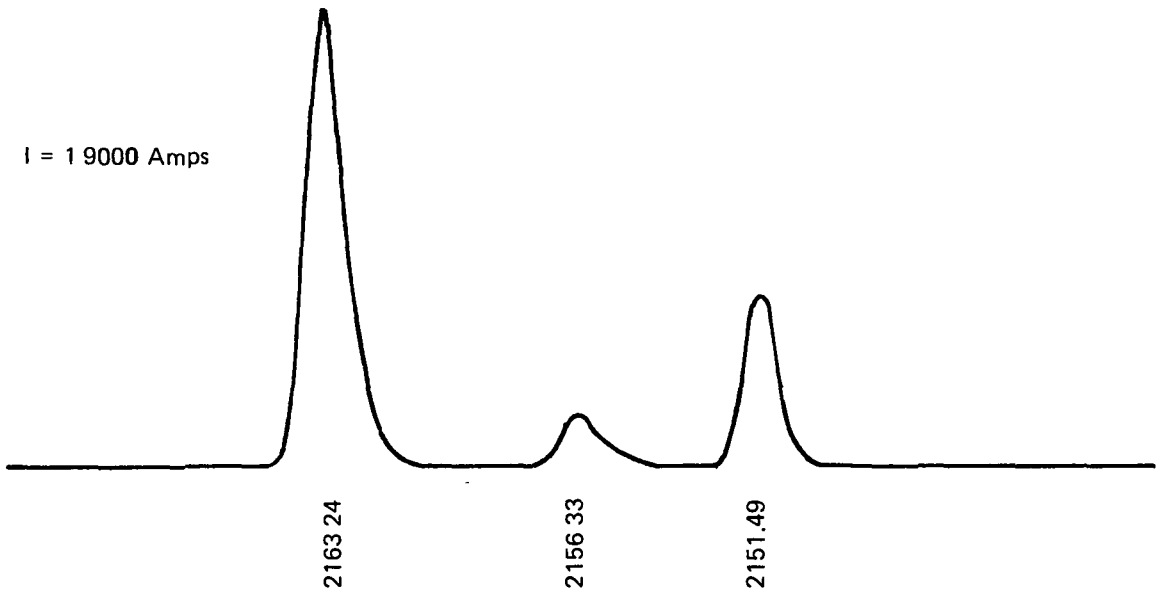

FIGURE 3–3 EMISSION SPECTRUM OF PbS Se TDL–08134–6. HORIZONTAL SCALE IS IN UNITS OF cm^{-1}.

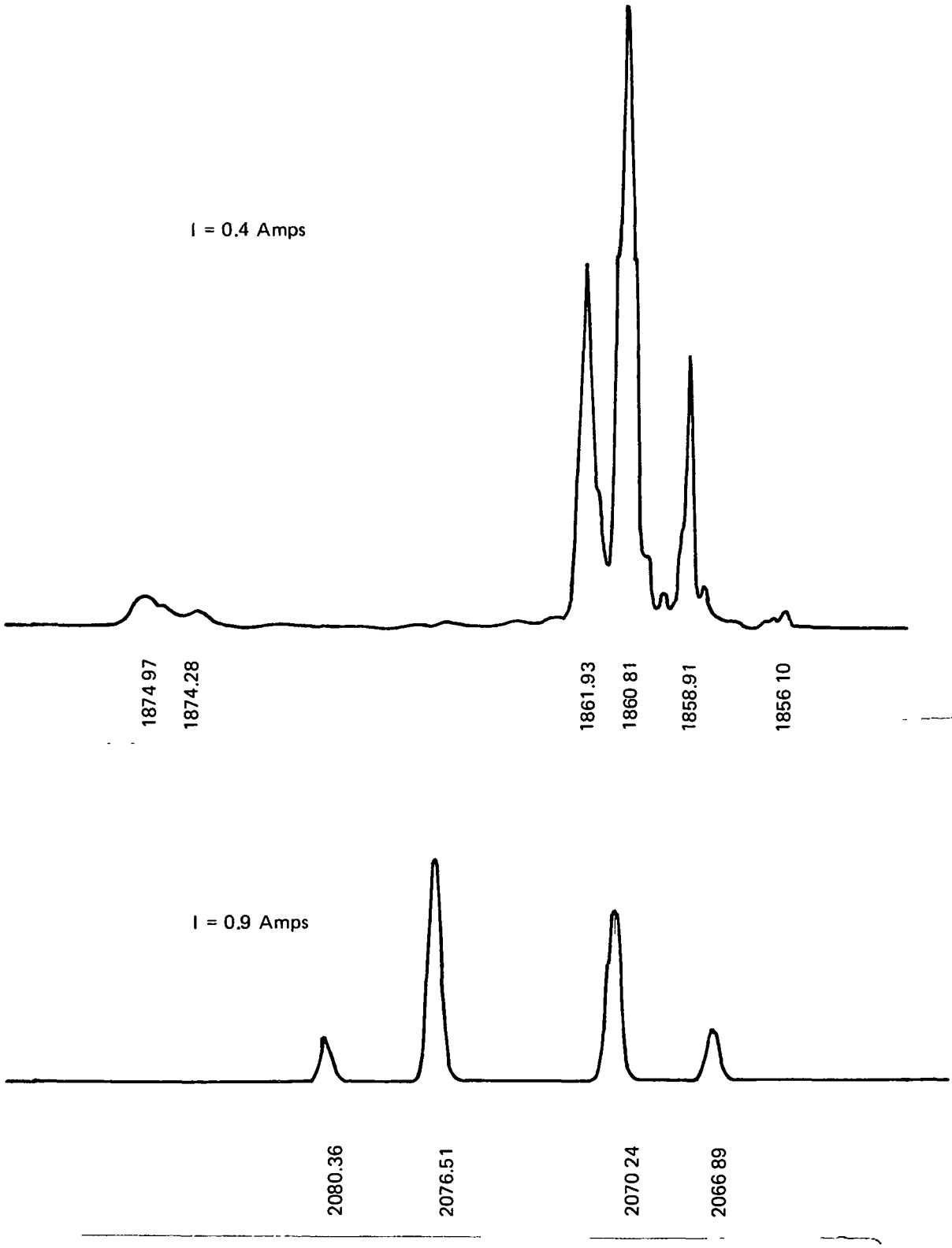

FIGURE 3–4 EMISSION SPECTRA OF TDL 08094–16. HORIZONTAL SCALE UNITS ARE cm^{-1}.

varies in magnitude considerably from one device to another. The electrical resistance was not evaluated in the devices reported here but it is reasonable to assume that it has a higher-than-average value in TDL-08094-16, leading to the observed heating effects. Note that at maximum power the external quantum efficiency of TDL 08094-16 (taking radiation from both ends into account) is about 9%.

The far-field spatial distribution in the plane of the junction was measured for an angle-lapped device and a standard device (F 3-5) by rotating the devices about their center line with the detector held fixed. Results are shown in F 3-5a and F 3-5b for a standard laser and an angle-lapped laser, respectively. The standard laser exhibits a complex spatial profile with two major lobes separated by about 60^{o}, while the angle-lapped device shows the well-defined, forward-directed lobe expected for a truly longitudinal cavity. The angular width of about 0.1 radian in the second case corresponds to a diffracting slit of about 50 μm width, or approximately 40% of the diode end-face. The structure associated with the standard laser can be qualitatively understood on the basis of a theory of Laff et al[11]. The following relationship follows from this theory:

$$\sin \frac{\theta}{2} = n \sin \left(\tan^{-1} \frac{2}{RN}\right) \qquad (3\text{-}1)$$

where θ is the angular distance between the two major lobes, n is the refractive index of the laser material, R is the length-to-width ratio of the laser and N is an order number. While n is not known for $PbS_{0.8}Se_{0.2}$, it can be estimated by a linear interpolation between the known values[12] for PbS and PbSe as 4.4. For TDL-08134-1, $R \simeq 4$. Using these values and the observed value of $\theta \simeq 64°$ in Equation (3-1) gives $N \simeq 4$. The value $N \simeq 4$ implies four, rather than the observed two main lobes; however the laser mounting package obscures radiation at an angle greater than about 120^{o}. The sharp substructure observable in the emission pattern may be due to diffraction effects at the package edge.

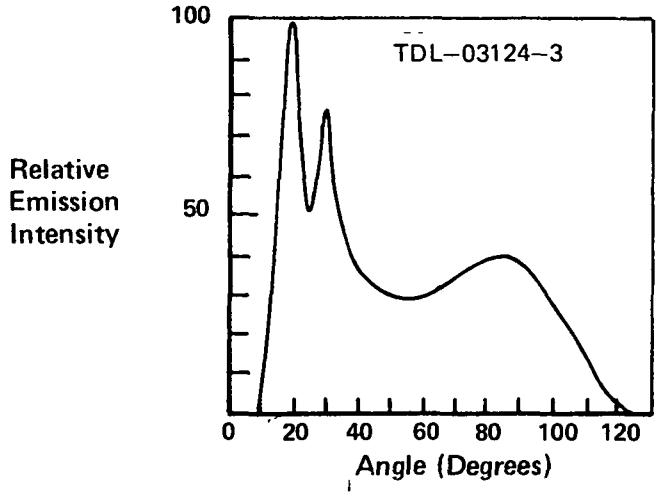

FIGURE 3–5a FAR-FIELD SCAN OF A CONVENTIONAL $PbS_{0.8}$ $Se_{0.2}$ DIODE LASER

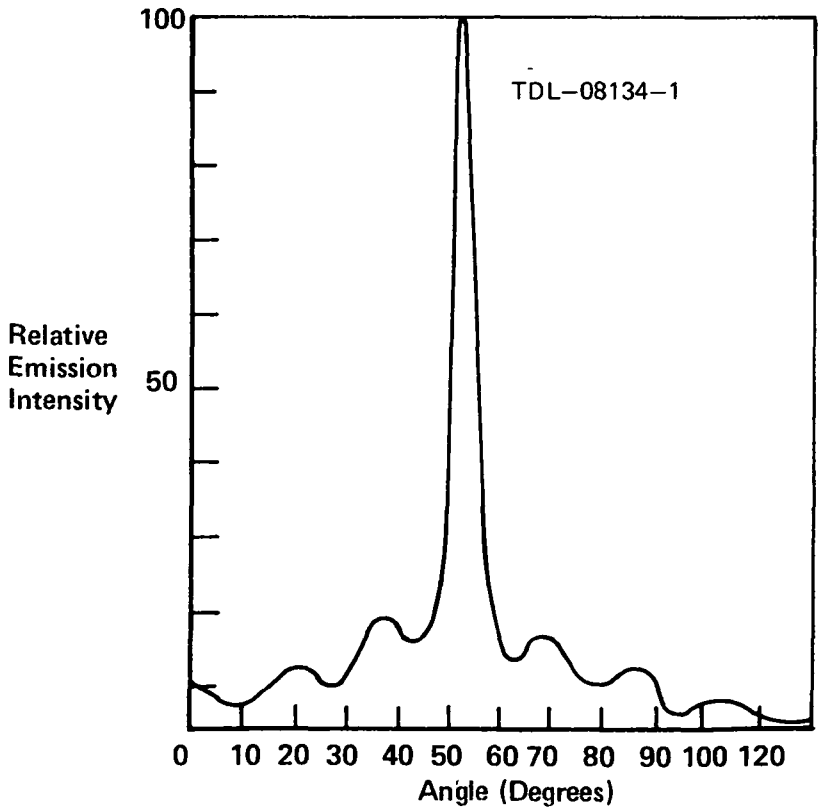

FIGURE 3–5b FAR-FIELD SCAN OF AN ANGLE-LAPPED $PbS_{0.8}$ $Se_{0.2}$ DIODE LASER

3.2 Optimization of pn-Junction Depth

In Section 2.4 we noted that a wide tuning range and high tuning rate in diode lasers could result from a deep pn-junction, but that such a condition is not desirable for applications, such as pollution monitoring, where an essentially fixed emission frequency is needed. For these applications, a shallow junction providing a more efficient heat transfer mechanism is desirable. Other considerations related to the pn-junction depth and profile are that a high carrier concentration and narrow depletion width are favorable from the viewpoint of both optical reabsorption and mode confinement, and that a high carrier concentration in the skin region is desirable to ensure that carrier injection is primarily from the skin region into the bulk rather than vice versa.

According to the studies of Brodersen et al related to interdiffusion in PbSe[13], an n-into-p diffusion should be significantly more favorable than a p-into-n diffusion for producing the desired thin, highly doped skin. Since diffusion parameters for PbSSe do not differ markedly from those of PbSe, we can expect the same considerations to apply to the former. Accordingly, samples of PbSSe which were n-type after the standard growth/annealing process were subjected to a further annealing step to convert them to p-type, and an n-skin was subsequently formed by diffusion.

In the first attempt, samples of CT58 ($x = 0.2$) were annealed at 600°C in the presence of an Se-saturated PbSe source for a period of three days. The crystals were converted to p-type as expected; according to the results of Strauss and Harman[8], the resulting hole concentration should have been on the order of 10^{19} cm^3. An n-skin was then formed by heating the crystal in the presence of a Pb-saturated PbSe source at 600°C for one hour. Stripe geometry diode lasers fabricated from these samples (Section 3.3) showed two noteworthy features. First, the overall tuning range was substantially lower than those of previous devices, as desired; for a typical device the range was 26 cm^{-1} (0.2 to 1.0 ampere) compared to nearly 100 cm^{-1} for earlier units. Second, the emission wavelength was 6.9 μm instead of the 4.7 μm observed with lasers

previously fabricated from the same crystal. We tentatively concluded and later verified that the annealing and diffusion process which utilized PbSe sources caused an increase in the Se/S ratio.

In the second attempt at junction profile optimization, a sample of CT58 was annealed at 600°C for three days in the presence of a $PbS_{0.8}Se_{0.2}$ vapor source saturated with $S_{0.8}Se_{0.2}$. An n-skin was then formed by heating the crystals at 525°C in the presence of an S-saturated PbS source for one hour. Stripe geometry lasers fabricated from this material exhibited the correct emission wavelength of 4.7 μm. The overall current tuning range (0.1 to 2.0 ampere) for a typical device was 17 cm^{-1}.

In a third experiment a crystal of CT66 (x = 0.385) was p-annealed at 600°C for three days using a vapor source consisting of stoichiometric $PbS_{0.615}Se_{0.385}$ with 1% by weight of pure Se added. The junction diffusion was performed at 525°C for one hour using an S-saturated PbS source. In this case (Section 3.3), the stripe geometry lasers had emission wavelengths of 5.9 μm, instead of 5.3 μm, indicating a composition change. A typical overall tuning range (0.25 to 2.0 ampere) was 12 cm^{-1}.

3.3 Stripe Geometry Diode Lasers

Depositions of a diffusion mask to form a barrier in the pn-junction diffusion process is an essential step in stripe geometry fabrication. Initial attempts at developing a suitable mask for the present program were directed toward using a SiO_2 layer, for which a silane deposition system with substrate heating facilities was assembled. However, substrate temperatures above 400°C were required to obtain a reproducible, well-adhering laser and stoichiometric changes and unavoidable contamination occurred at these temperatures. Films deposited at lower temperatures generally lifted during the diffusion step and thus did not provide effective masking. Subsequent attempts to use evaporated ZnS as the diffusion mask were unsuccessful because the ZnS acted as a source of acceptor impurities.

Evaporated MgF_2 provided a tenacious, non-doping layer, but the relatively high temperature required for thermal evaporation of this material caused an undesirable heating of the crystal. The apparent solution was to use an electron beam system to evaporate MgF_2 without significantly heating the substrate. The electron beam facilities were not available within the ADL laboratories, and arrangements were made to have this step performed at MIT Lincoln Laboratory. The MgF_2 evaporation was carried out through a "finger" mask to produce an MgF_2 layer with 0.002-inch-wide open stripes. Good quality MgF_2 films of 0.2 μm thickness were deposited without difficulty.

Stripe geometry lasers in this program were fabricated from p-type crystals formed by type conversion. The MgF_2 diffusion masks were deposited on cleaved or polished surfaces and n-skins formed in the open stripes by diffusion. After diffusion, the crystals were lapped to a thickness of approximately 150 μm and Au/Pt/In layers deposited on both surfaces. Individual devices were then formed by cleaving. (F 3-6 illustrates the stripe geometry laser construction.) Several of the stripe geometry lasers were mounted in improved packages (see Section 3.6).

Operating characteristics of representative stripe geometry lasers are described in the following paragraphs:

- TDL S58-1X: This device was fabricated from a crystal of CT58 ($x = 0.20$) which had been type-converted using a Se-saturated PbSe source (as described in Section 3.2). It was assembled in the new package described in Section 3.6.

  A representative emission spectrum for S58-1X is shown in F 3-7. The emission wavelength of 6.9 μm is considerably displaced from the value of 4.7 μm expected for this composition. This unexpected result was believed to be due to the high-temperature conversion anneal carried out with a PbSe vapor source; subsequent results confirmed this hypothesis. The overall

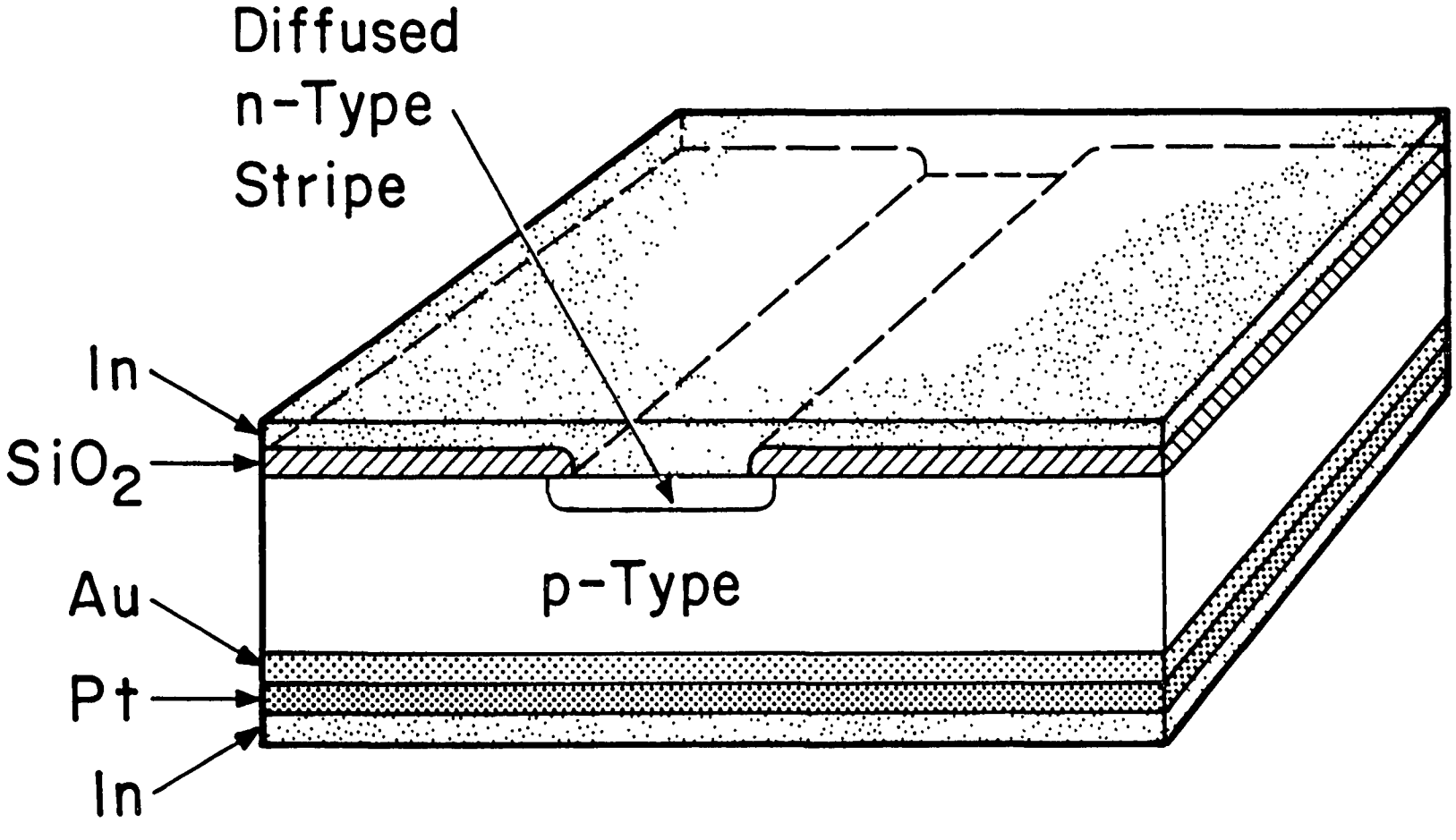

FIGURE 3–6 CONCEPTUAL DRAWING OF THE STRIPE GEOMETRY DIODE CONFIGURATION.

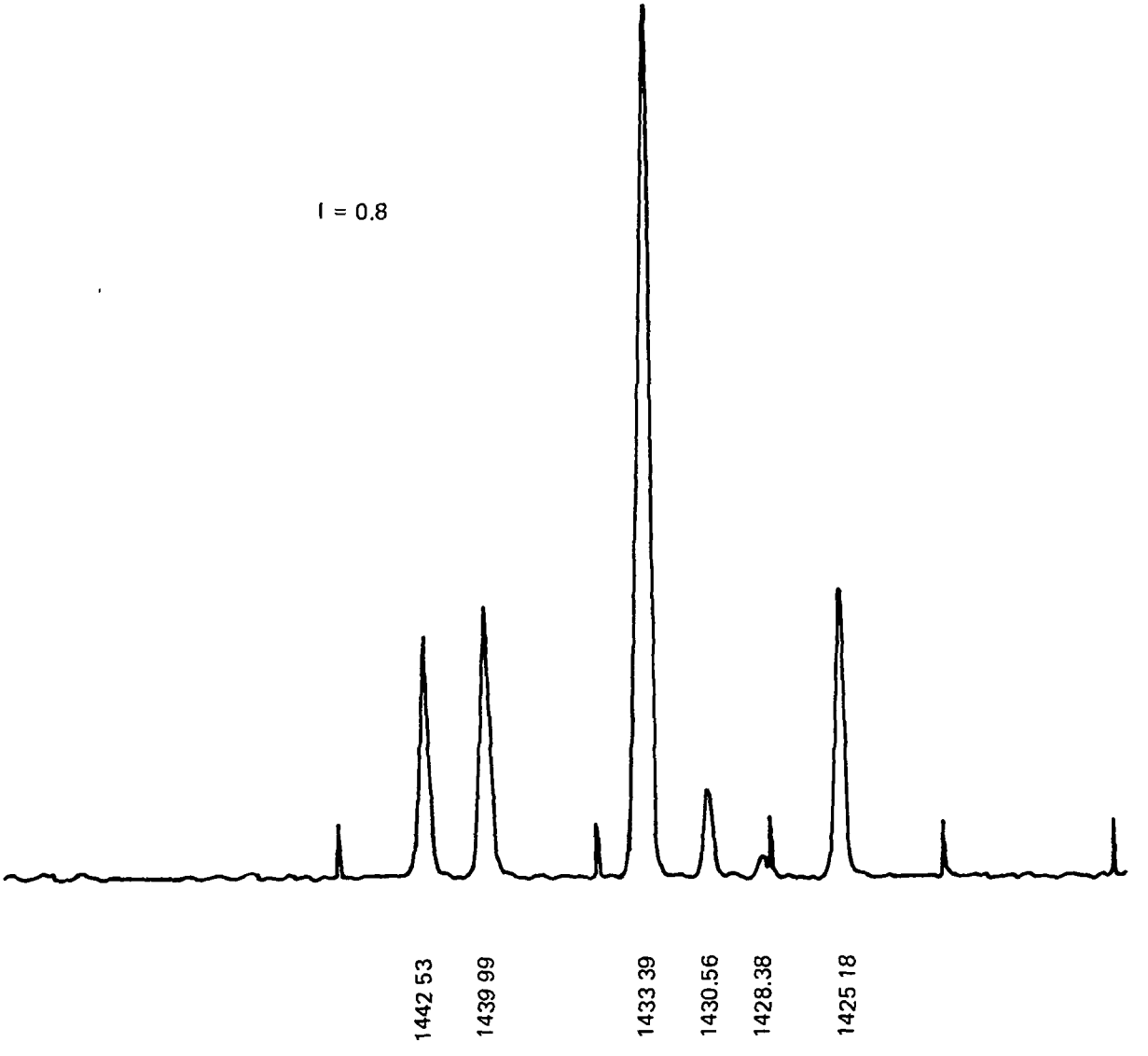

FIGURE 3–7 EMISSION SPECTRUM OF TDL S58-1X

tuning range of this device was about 26 cm^{-1}. This tuning range is considerably less than that of the diode described in Section 2.5 and is believed to reflect the much shallower pn-junction in the present case.

Single-ended power output as a function of diode current is shown in F 3-8. The maximum single-mode power output is 3 milliwatts.

- TDL S58-2X: This device was fabricated from a crystal which was p-converted by the second method described in Section 3.2; that is, the vapor source had the same composition in all respects as the crystal. The n-skin was formed at the somewhat lower diffusion temperature of 525°C. This device was also assembled in the improved package.

F 3-9 presents a series of emission spectra measured at various current levels. The relative intensities in these various spectra are of no significance since the amplifier gain was adjusted to maintain an approximately level output as the signal intensity increased. The emission occurs in one principal mode with at most three small satellite modes for currents up to five times threshold. In the vicinity of 1 ampere, the emission becomes distributed into a larger number of evenly spaced modes, but at higher currents again becomes concentrated into a few modes. The mode structure quality begins to deteriorate in the vicinity of 2 ampere. The emission wavelength is in the vicinity of 4.7 μm, as expected, and the overall tuning range (0-2 ampere) is 23 cm^{-1}. Plotting single-ended power output vs. bias current for S58-2X (F 3-10) shows that the maximum value

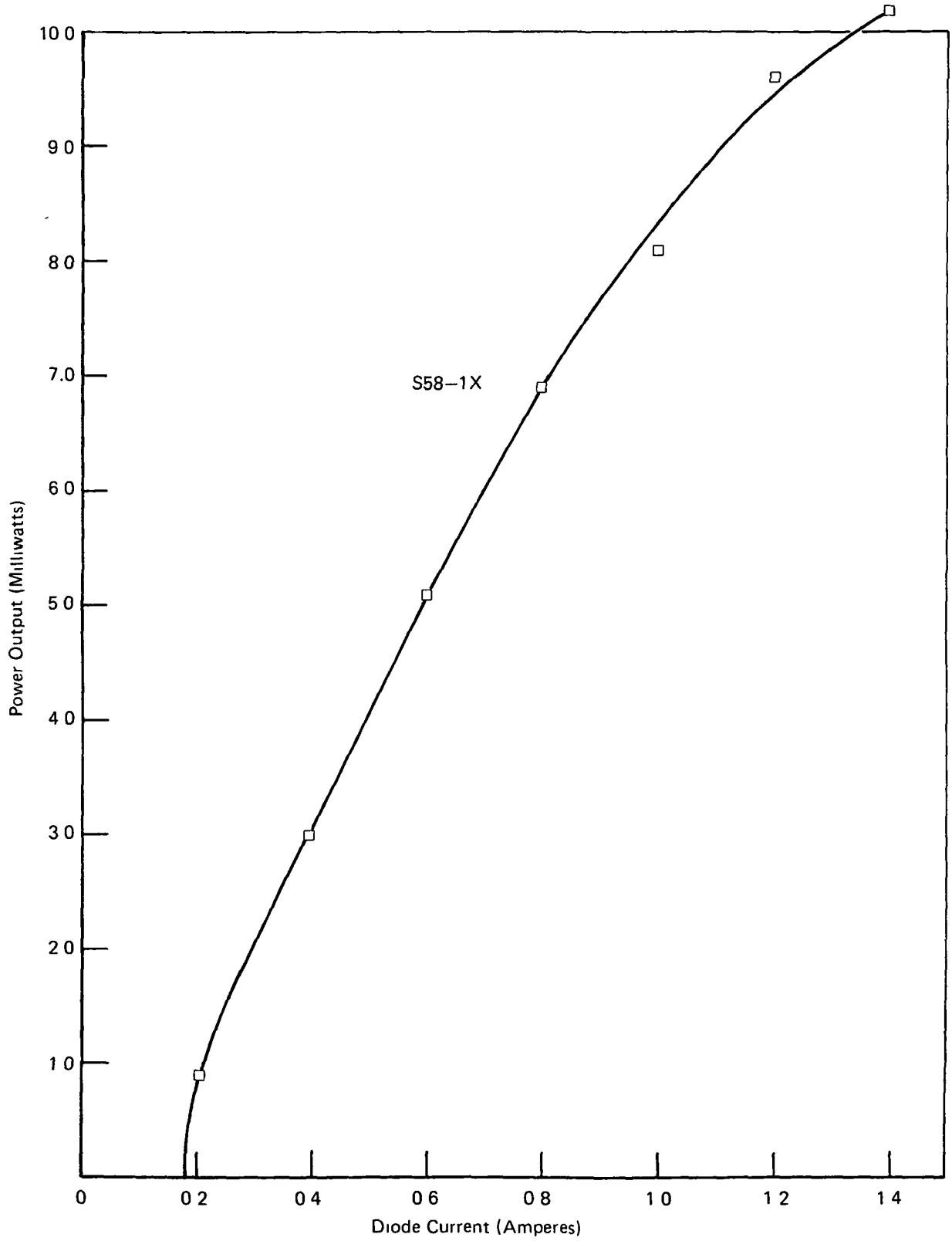

FIGURE 3–8 DEPENDENCE OF SINGLE-ENDED, CW OUTPUT POWER ON BIAS CURRENT FOR TDL S58-1X

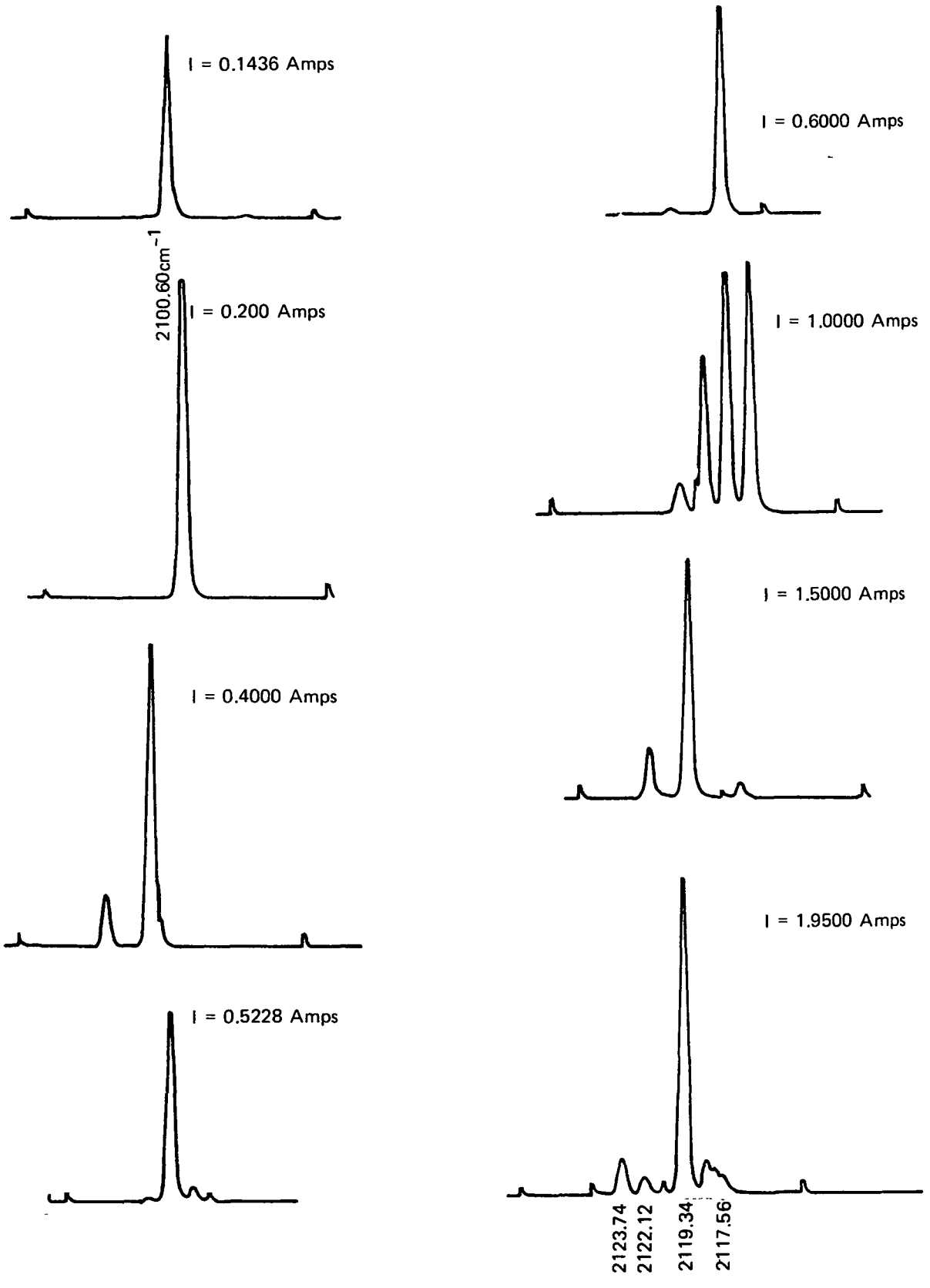

FIGURE 3–9 EMISSION SPECTRA AT VARIOUS BIAS CURRENTS FOR TDL S58-1X.

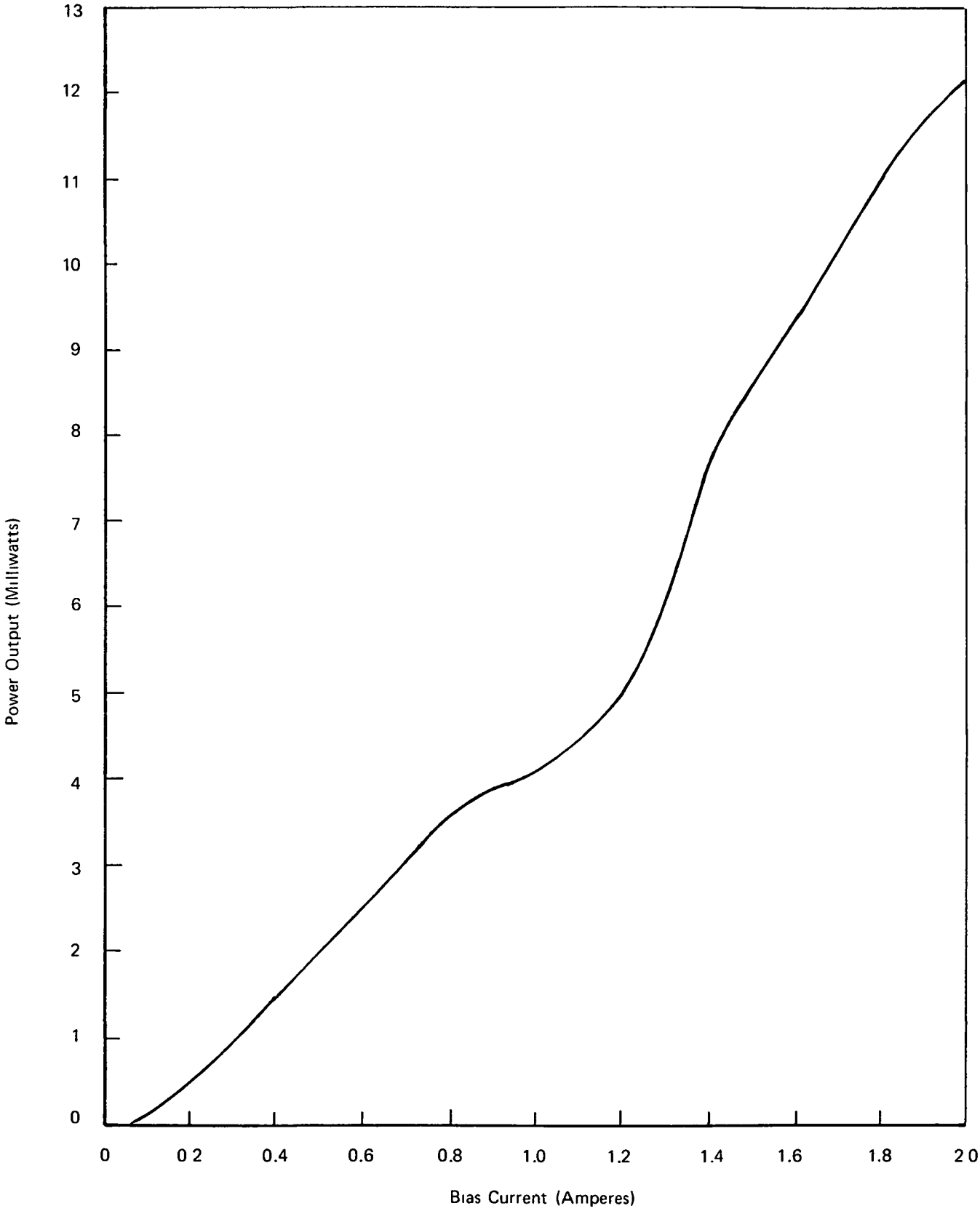

FIGURE 3–10 DEPENDENCE OF SINGLE-ENDED, CW OUTPUT POWER ON BIAS CURRENT FOR TDL S58-2X

is 12.2 milliwatts. It may be deduced from F 3-9 that over 70% of the power at 2 ampere is concentrated in a single mode, implying a maximum single mode power greater than 8.4 milliwatts from one end of the laser.

- TDL S66-1X: This laser was fabricated from material resulting from the third p-conversion experiment described in Section 3.2. The source for the conversion anneal was a stoichiometric crystal of the correct composition (x = 0.385), to which had been added 1% by weight of Se. The laser was mounted in the improved package.

  A representative emission spectrum (F 3-11) shows that the emission occurs near 5.9 μm instead of 5.3 μm. This shift is ascribed to a compositional change resulting from the excess Se added to the conversion anneal vapor source.

  The maximum observed single-ended output power for S66-1X was 7.8 milliwatts, measured at a bias of 2 ampere. According to the spectral data, this corresponds to a single-mode power from one end face of 5.7 milliwatts.

3.4 End Face Metallization

In the standard fabrication procedure for diode lasers both end faces have equal transmission, although radiation from only one face is used; radiation out of the back face is discarded. It was thus expected that rendering the back surface completely reflective would decrease the threshold current and increase the power out of the front surface. To investigate this possibility, several angle-lapped lasers were fabricated in the usual manner and, after evaluation, 2000Å insulating layers of MgF_2, followed by 3000Å reflective layers of Au were deposited on the back surfaces. The pulsed threshold currents and power outputs were

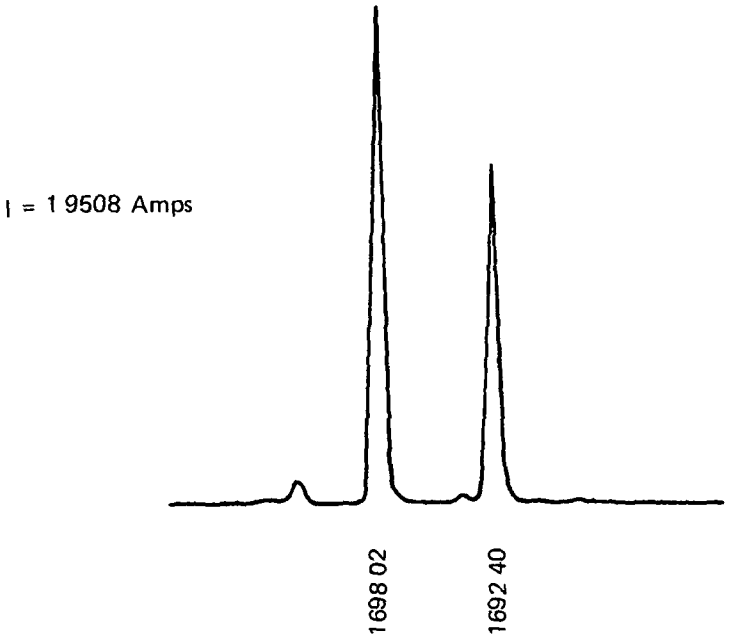

FIGURE 3–11 EMISSION SPECTRUM FOR TDL S66-1X

evaluated before and after these depositions. The goals of this effort were both to achieve improved device performance and to obtain fundamental information concerning the loss and gain parameters of the lasers.

Improvements in diode laser performance were expected from the following consideration. The threshold current density J_{th} and external quantum-efficiency, η_e, are related to laser parameters as[14]

$$J_{th} = \frac{1}{\beta \ell} \left[\alpha \ell + \frac{1}{2} \ln \left(\frac{1}{R_1 R_2} \right) \right] \tag{3-2}$$

$$\eta_e = \eta_i \frac{\ln \left(\frac{1}{R_1} \right)}{2\left[\alpha \ell + \frac{1}{2} \ln \left(\frac{1}{R_1 R_2} \right)\right]} \tag{3-3}$$

where α and β are the loss coefficient and gain factor, respectively, ℓ is the cavity length, R_1 and R_2, the end-face reflectivities, and η_i, the internal quantum efficiency. For unmetallized diodes, the end faces have equal reflectivities, determined by the dielectric constant of the material, and are approximately, $R_1 = R_2 = 0.5$. With one end face metallized, $R_1 = 0.5$ and $R_2 = 1$. Adding subscripts u and m to denote the unmetallized and metallized cases respectively then,

$$J_{thu} = \frac{1}{\beta \ell} \left[\alpha \ell + \ln \left(\frac{1}{R} \right) \right] \tag{3-4a}$$

$$J_{thm} = \frac{1}{\beta \ell} \left[\alpha \ell + \frac{1}{2} \ln \left(\frac{1}{R} \right) \right] \tag{3-4b}$$

$$\eta_{eu} = \eta_i \frac{\ln \left(\frac{1}{R} \right)}{2\left[\alpha \ell + \ln \left(\frac{1}{R} \right) \right]} \tag{3-5a}$$

$$\eta_{em} = \eta_i \frac{\ln \left(\frac{1}{R} \right)}{2\left[\alpha \ell + \frac{1}{2} \ln \left(\frac{1}{R} \right) \right]} \tag{3-5b}$$

The above equations indicate that the effect of metallizing one end face is to reduce the quantity $\ell n \left(\frac{1}{R} \right)$ to $\frac{1}{2} \ell n \left(\frac{1}{R} \right)$. Any improvement in operating characteristics should thus depend on the relative magnitude of the internal loss term $\alpha \ell$ with respect to the reflective loss term $\ln \left(\frac{1}{R} \right)$.

Threshold currents and power outputs were measured with the lasers immersed in liquid He. Measurements were made on a pulse basis, using 2 microsecond pulses at a 10^3 Hz repetition rate to eliminate beating effects. As discussed below, beating may be a significant factor. Results are shown in Table 3-2, along with values of α and β calculated from the pair of simultaneous Equations 3-4.

While pulse threshold currents were reduced considerably by end-face metallization as expected, it was found that the devices would not operate in the CW mode after metallization; CW operation was easily achieved before metallization. The cause of this adverse effect is not known. It may be due to strains induced in the laser crystals by the evaporation process, since the lasers are unavoidably heated to some extent during the process. Another possible explanation is that internal heating due to electromagnetic energy within the laser cavity is higher in the metallized devices and might act to quench laser action. Clearly additional work is needed to explain this phenomenon.

It is of interest to consider what performance levels could be achieved with one metallized end face and the opposite end-face with an anti-reflection coating which reduces the reflectivity to, say, $R_2 = 0.1$. For this calculation, the average parameter values from Table 3-2, $\overline{\alpha \ell} = 0.13$ and $\overline{\beta \ell} = 1.3 \times 10^{-3}$ can be used in Equations 3-2 and 3-3. This gives $J_{th} = 985$ A/cm^2 and $\eta_e = 0.89\ \eta_i$. This result indicates that high power outputs are potentially attainable, since the earlier discussion related to F 2-9 indicated high internal quantum efficiencies. For $\eta_i = 1.0$ in this case, the CW output power is calculated to be 221 milliwatts for 5 μm radiation and a bias current of 1.0 ampere.

TABLE 3-2

RESULTS OF END-FACE METALLIZATIONS

	TDL 08134-3	TDL 08123-4	TDL 08094-14	TDL 08144-2
ℓ (cm)	0.024	0.020	0.019	0.020
J_{thu} (A/cm^2)	550	350	560	500
J_{thm} (A/cm^2)	320	220	320	320
α (cm^{-1})	7.0	5.1	5.4	8.2
β (cm/amp)	0.062	0.060	0.075	0.061

3.5 End Face Polishing

Walpole et al[15] have reported that the output power from PbSnTe lasers could be considerably improved by using polished rather than cleaved end faces. They ascribed the improvement to the elimination of surface roughness which, on cleaved surfaces, varied from greater than 0.1 μm in the best cases to several μm on the poorest surfaces. These dimensions are comparable to the internal wavelength of emission for the PbSnTe lasers studied (about 1.6 μm).

In the present program, we investigated end face flatness of PbSSe lasers by standard interference microscopy, using the green line of a low-pressure Hg vapor lamp. For these measurements, the laser crystals were removed from the packages and wax-mounted on microscope slides. We found that lasers from crystals exhibiting good cleaving properties were flat to within the resolution of the measurement ($\lesssim$ 0.1 μm) over essentially their whole end face.

On the other hand, lasers from crystals which did not cleave easily showed surface irregularities of 1 μm or more. For comparison, the internal wavelength of emission for the lasers in this program is approximately 1 μm.

An etch-polishing technique similar to that for angle-lapping lasers was used to produce polished end faces that were flat to within the measurement resolution for all crystals studied. With a number of crystals, comparison tests were made in which both cleaved-face and polished-face lasers were fabricated and evaluated. In crystals with good cleaving properties there was no noticeable difference between the two types of device. Crystals which did not cleave well showed poor device performance (threshold current densities greater than 1,000 amp/cm^2, typically) for both cases, suggesting that the performance is limited by internal bulk effects rather than surface flatness.

Thus, we concluded that PbSSe laser performance was not significantly improved by end face polishing and this step was therefore not incorporated into the fabrication process.

3.6 Investigation of Packaging Damage

In the standard ADL packaging method, electrical contact to the top surface is made with a "C-bend", an In-plated, Be-Cu wire spring loaded to the top of the laser crystal. The In-In cold weld between the laser crystal and the C-bend provides a reliable, mechanically rigid bond. However, there has been concern that the localized pressure exerted by this type of contact damages the laser crystal. To investigate this possibility, several laser assemblies were dismantled and their metal layers removed by chemical etching. The crystals were cleaved through the point of contact with the C-bend, allowing microscopic observation of the cross-sectional regions below.

A typical example of the results (F 3-12) clearly shows that the C-bend deforms the crystal at the point of contact: the depression is approximately 20 μm deep. Etch pit densities in the order of 10^8 cm^{-2} were observed in the vicinity of the depression.

The active pn-junction region is near the opposite side of the crystal, and further observations were made to determine if the C-bend damage propagates into this region. Evidence that such propagation does occur is shown in F 3-13. The small, square region is a hillock, approximately 5 μm in height, with its side oriented along (100) crystal axes. The hillock is directly beneath the point of C-bend contact, although on the opposite side of the 0.025-cm-thick crystal. Similar hillocks were observed on nearly every device investigated.

The undesirable effects of the observed deformation may include a reduction in quantum efficiency due to nonradiative recombination in damaged regions of the crystal and deformation of the laser cavity. It appears that the C-bend contact, although excellent in terms of mechanical strength and rigidity, may be a source of laser degradation. In view of this problem, an improved diode laser package was investigated. Suggestions of Dr. K. W. Nill of MIT Lincoln Laboratory led to the assembly of an improved package in which both top and bottom contacts are made uniformly on the crystal surfaces, greatly reducing or eliminating localized

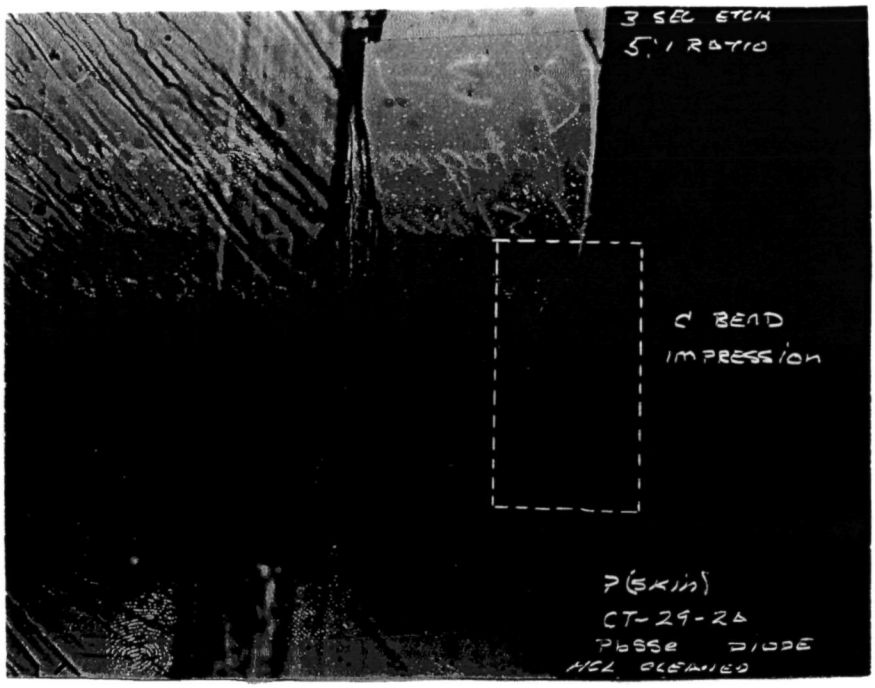

FIGURE 3–12 CRYSTAL DEFORMATION DUE TO C-BEND CONTACT: ADJACENT TO C-BEND.

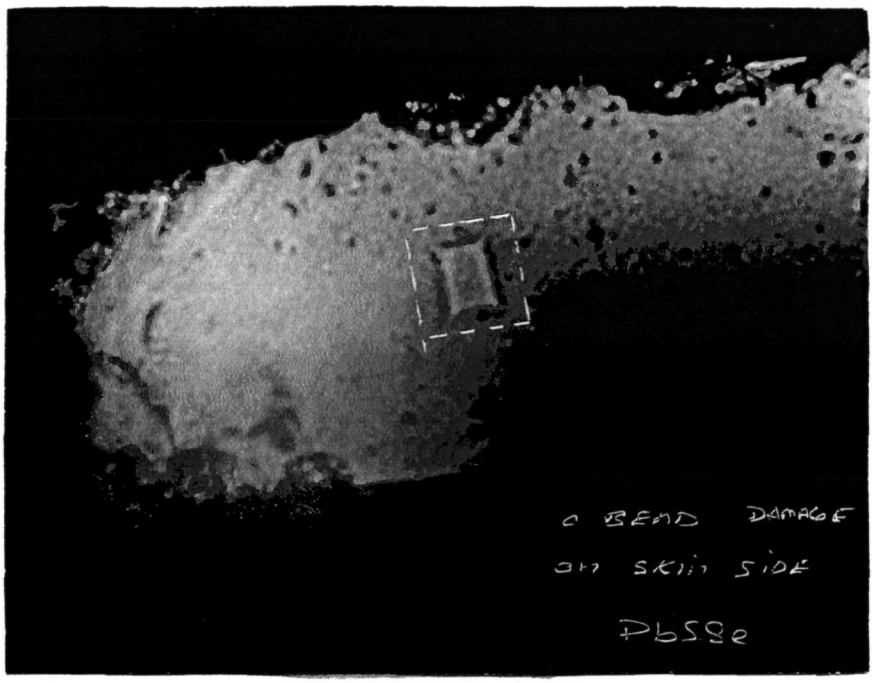

FIGURE 3–13 **CRYSTAL DEFORMATION DUE TO C-BEND CONTACT: ON OPPOSITE CRYSTAL FACE**

pressure on the crystal. The package also provides superior heat sinking by allowing efficient heat flow out of the top surface. (The top contact is thermally connected to the base through electrically insulating spacers.) Several of the lasers supplied to NASA Langley Research Center were delivered in the improved packages.

SECTION 4

CONCLUSIONS AND RECOMMENDATIONS

The principal result of this program was the achievement of a substantial increase in output power through the development of improved fabrication methods. The goal of 1 milliwatt of CW, single-mode, single-ended power output, was achieved, with exceptional devices exhibiting values greater than 8 milliwatts. The experimental results related to end face metallization indicate that even greater improvement in output power should be attainable. Theoretically, an external quantum efficiency of 70% corresponds to a CW output power of about 350 milliwatts at 2 ampere.

It was found that the current tuning rate could be controlled by adjusting the pn-junction depth. This allows tuning rates to be optimized for particular applications. Thus, a rapid tuning rate with wide range may be preferable for general spectroscopic laboratory studies, whereas a slow rate may be desired for monitoring applications where a fixed frequency is maintained.

An unexpected phenomenon was enocuntered when crystal composition was observed to be significantly altered by annealing at temperatures as low as 600°C. The composition was changed by transport of material through the vapor phase. This effect caused unexpected problems in achieving diode lasers with the desired operating characteristics, and is highly significant with respect to Pb-salt device fabrication.

It was discovered that the present method of packaging introduces gross damaging effects in the laser crystal through pressure applied by the C-bend. While there was no direct evidence that this damage affected laser performance, it is well known that dislocation and other lattice imperfections induced by such damage can be significant sources of non-radiative recombination. Furthermore, the stress-induced distortion of the laser cavity should lead to further inefficiencies.

The results of this investigation suggest a number of directions for future work. The following tasks are suggested as potentially fruitful, direct follow-ons of the present effort.

a) Junction profile optimization. Preliminary results in this work showed that substantially higher output power was achieved in the p-skin configuration as compared to the n-skin configuration. This is believed to be due to the steeper junction profile attainable with the former structure. Further annealing and diffusion studies should be carried out to further optimize the concentration profile and levels.

b) End face metallization. Results showed that improved performance could be attained by depositing a thin-film Au mirror on one end face, but that an unexplained degradation effect subsequently prevented CW operation. This degradation should be further investigated and, hopefully, eliminated to allow further use of end face metallization.

c) Anti-reflection coatings. Results of end face metallization studies indicated a substantial increase in output power can be achieved by depositing an anti-reflection coating on one end face. This possibility should be studied experimentally.

d) Contact effects. Contact resistance should be studied in detail in respect to device performance and fabrication procedures. Alternative metal contacts and surface preparation techniques should be further investigated.

e) Laser characterization. Properties such as noise in the output emission, mode stability and spatial profile of emission (including phase) should be investigated in detail.

f) Lifetime. Shelf lifetime, operating lifetime and effects on lifetime of temperature cycling should be characterized.

Acknowledgement

Evaporations of diffusion masks for stripe geometry formation were performed by Dr. K. W. Nill of the Massachusetts Institute of Technology Lincoln Laboratory.

SECTION 5

REFERENCES

1. Frank Allario, R. K. Seals, Jr., Philip Brockman, and R. V. Hess: "Tunable Semiconductor Lasers and Their Application to Environmental Sensing." Paper presented at the 10th Anniversary Meeting of the Society of Engineering Science, Raleigh, North Carolina, November 5-7, 1973. To be published in "Recent Advances In Engineering Science," Vol. 6, Oct. 1975, Science Publishers, Boston, Massachusetts.

2. R. K. Seals, Jr.: "Analysis of Tunable Laser Heterodyne Radiometry: Remote Sensing of Atmospheric Gases." AIAA J., Vol. 12, No. 8, August 1974, pp. 1118-1122.

3. Philip Brockman and R. K. Seals, Jr.: "Analysis of Laser Measurement of High-Altitude Aircraft Emissions." AIAA J., Vol. 12, No. 5, May 1974, pp. 651-655.

4. R. K. Seals, Jr. and C. H. Bair: "Analysis of Laser Differential Absorption Remote Sensing Diffuse Reflection From the Earth," publication of the Instrument Society of America, ISA, JSP, 6675, 1973.

5. G. W. Sachse et al: "Airborne Tropospheric Carbon Monoxide Monitor Using a Tunable Diode Laser (Instrument Concept)." Presented at Fourth Annual Remote Sensing of Earth Resources Conference, University of Tennessee Space Institute, Tullahoma, Tenn.

6. R. K. Seals, Jr. and B. J. Peyton: "Remote Sensing of Atmospheric Pollutant Gases Using an Infrared Heterodyne Spectrometer." Paper presented at the International Conference on Environmental Sensing and Assessment, Las Vegas, Nevada, September 14-19, 1975.

7. For a review, see E. D. Hinkley et al: "Infrared Spectroscopy with Tunable Lasers." Topics in Applied Physics, Vol. 2, H. Walther, Ed., New York, Spring 1975.

8. A. J. Strauss and S. Harman, MIT Lincoln Laboratory Solid State Research Report, 1972:4, p. 31.

9. J. F. Butler et al, Appl. Phys. Lett 5, 75 (1964).

10. K. W. Nill et al in "Physics of IV-VI Compounds and Alloys," S. Rabii, Ed., Gordon and Breach, New York, 1974, pp. 25-30.

11. A. Laff et al, IBM J. Res. and Devel. 7 63, 1963.

12. J. N. Zemel et al, Phys. Rev. 140, A330, 1965.

13. R. W. Brodersen, J. N. Walpole and A. R. Calawa, J. Appl. Phys. 41, 1484, 1970.

14. J. I. Pankove: "Optical Processes in Semiconductors," Prentice Hall, Englewood Cliffs, 1971, p. 215.

15. J. N. Walpole, A. R. Calawa, R. W. Ralston, and T. C. Harman, J. Appl. Phys. 44, 2905, 1973.

LIST OF FIGURES

LIST OF TABLES